TABLE OF CONTENTS

LIST OF TABLES

LIST OF FIGURES

1.0 INTRODUCTION

1.1 PURPOSE

The development of the Emergency Assessment and Response System (EARS) at the San Onofre Nuclear Generating Station (SONGS) is in response to the Nuclear Regulatory Commission's recent upgrading requirements concerning preparedness for radiological emergencies at operating nuclear power plants. As part of this system, site-specific, real-time estimates of ambient radionuclide concentrations are needed in response to the requirements of NUREG-0654, "Criteria for Preparation and Evaluation of Radiological Emergency Response Plans and Preparedness in Support of Nuclear Power Plants," Appendix 2. This report presents the results of a site-specific study and system development that upgrades the transport and dispersion portion of the EARS at SONGS.

The present operation of the EARS involves the use of 15-minute averages of meteorological data, from the Bluff Meteorological Tower System, as input to a segmented plume transport and dispersion model. Model calculations of transport and dispersion from SONGS are based on the assumption that the bluff tower meteorological observations apply uniformly throughout the area of interest surrounding the SONGS site. Uniform meteorological fields, particularly the wind field, are not realistic in this area because of the terrain surrounding the SONGS site and the affect of the land/sea interface on the flow characteristics. Greater realism in the EARS transport and dispersion assessment would result from the use of nonuniform meteorological fields in the segmented plume emergency release assessment program. The development of site-specific nonuniform meteorological fields for use in the emergency assessment system for SONGS is the purpose of this study

Because of the hardware and software limitations of the present EARS, the following tasks have been required for the development of the nonuniform meteorological fields for incorporation in the EARS transport and dispersion system:

1. Use historical meteorological data to generate nonuniform meteorological fields associated with specific important categories of meteorological observations at the SONGS bluff tower.

2. Format the nonuniform meteorological fields for use in the present configured EARS.

3. Develop an access system that identifies a specific meteorological field consisting of wind speed and direction, atmospheric stability, and mixing height fields, with every possible set of wind speed, wind direction, and atmospheric stability measured at the SONGS tower.

4. Generate a computer code that will, when incorporated in the EARS, identify and select the proper meteorological field for use under a set of real-time bluff meteorological measurements and perform any necessary scaling of the meteorological parameters prior to use in the radiological assessment.

1.2 STUDY REGION

SONGS is located on a coastal site, approximately 80 km southeast of Los Angeles in southern California. The coast line, oriented approximately in a northwest to southeast direction, divides the study region into roughly equal ocean and land areas. The study region is that area included within a square 50 km on a side, centered on the SONGS site.

The SONGS site itself is located adjacent to the shoreline, at the base of a bluff rising approximately 30 m to the level of the coastal highway (Interstate Highway 5) running between Los Angeles and San Diego. The SONGS meteorological tower is located on the bluff adjacent to the reactor site. Steep, undulating hills rise to more than 500 m above mean sea level (MSL) immediately east of the site, and to about 240 m MSL in all onshore directions (to the north and east) within 6 km of the site. The hills are cut by a number of deep canyons that lead inland from the coast.

The northeastern quadrant of the study region extends into the rugged Santa Margarita mountain range that has peaks rising above 900 m. A topographical map of the study region is given in Figure 1-1. This figure also shows the locations of meteorological stations used in this study. Figure 1-2 presents the actual 50-km square region used in this study including topography and locations of the meteorological stations. This figure can be used for direct comparison with the output wind fields of Appendix B.

The heterogeneity of the surface within the study region is apparent in Figure 1-1. Significant meteorological effects are associated with this surface heterogeneity, for example:

1. Diurnal coastal effects such as sea-breeze and land-breeze systems.
2. Rapidly-varying coastal effects associated with coastal internal boundary layers that result in differing atmospheric stability characteristics above the sea and land surfaces.
3. Channeling of wind flow by hills and canyons.
4. Up-slope and down-slope winds due to radiative heating and cooling of steep terrain.

Each of these effects tend to make the meteorological characteristics of the atmosphere in the study region nonuniform.

1.3 LIMITATIONS OF STUDY

The basic desired product of this study, because of the hardware and software limitations of the EARS, is a procedure by which real-time meteorological observations at the SONGS tower can be used to identify realistic and representative meteorological fields for use in dispersion and transport analysis throughout the study region. The most important, in terms of dispersion and transport analysis, and generally the most variable meteorological field is the wind field. Although reference is often made to the wind field in the remainder of this

section, the points raised and discussions generally also apply to the atmospheric stability and mixing height fields.

It should be recognized that the primary limitation of this study and wind field development methodology is the fact that the actual real-time meteorological fields for the region cannot be developed from data obtained from a single station. The goal of this study is to generate, within the limitations of the system and meteorological data, more realistic and representative meteorological fields for use in the dispersion and transport assessment. Both the development of the nonuniform meteorological fields from historical concurrent site and offsite data, and the categorization of these nonuniform fields for use on a real-time basis are constrained to the routinely available meteorological data in the EARS; the primary SONGS bluff tower meteorological measurements.

An example of the particular problem created with the limited historical meteorological data and single station real-time measurements is that, for some meteorological categories, significantly dissimilar nonuniform wind fields were obtained. That is, for a given season, time of day, wind direction, wind speed class, and atmospheric stability class (five characteristics that were eventually used to define the categories), a number of significantly different nonuniform meteorological fields were developed. In these cases, the more representative nonuniform meteorological field, in terms of frequency of occurrence, was selected for the category.

Historical meteorological data used in this study were from ten reporting stations in the region. These stations were of various types, including National Weather Service (NWS) stations, military weather observation stations, and meteorological monitors associated with air quality monitoring stations. The data from the various types of stations were obtained using different observational techniques, instrumentation quality and maintenance procedures, and different methods of atmospheric stability classification. The quality and completeness of the data varied from station to station.

Although this study was also limited by the amount of meteorological data (one-year period) and by the necessary subjective nature of certain judgements regarding the most representative nonuniform field for some categories, the nonuniform meteorological fields produced for use in the transport and dispersion analysis are realistic because they were based on actual observed concurrent meteorological data. Insofar as the nonuniform meteorological fields developed from the one-year historical data period are representative of the period during which the SONGS EARS will be operating, the developed meteorological fields can be considered representative of the categories to which they are assigned. However, no statement can be made about the accuracy with which a nonuniform wind field, generated by the procedure developed in this study, will model the actual wind field that will exist during any period in which the EARS is operating. The actual wind field during any future period may be of a type not observed during the one-year historical period on which this study was based, or may be of a type only infrequently observed and, therefore, not chosen as representative of the category. Alternatively, the use of uniform wind fields throughout the area, corresponding to the SONGS meteorological tower observations, is also inaccurate, and in general is unrealistic and unrepresentative as well. Therefore, the admitted limitations of the product of this study are less severe than those of the only available alternative technique. The use of the nonuniform meteorological fields in the transport and dispersion assessments for SONGS should provide more realistic and representative estimates of pollutant concentrations for use in emergency evaluations.

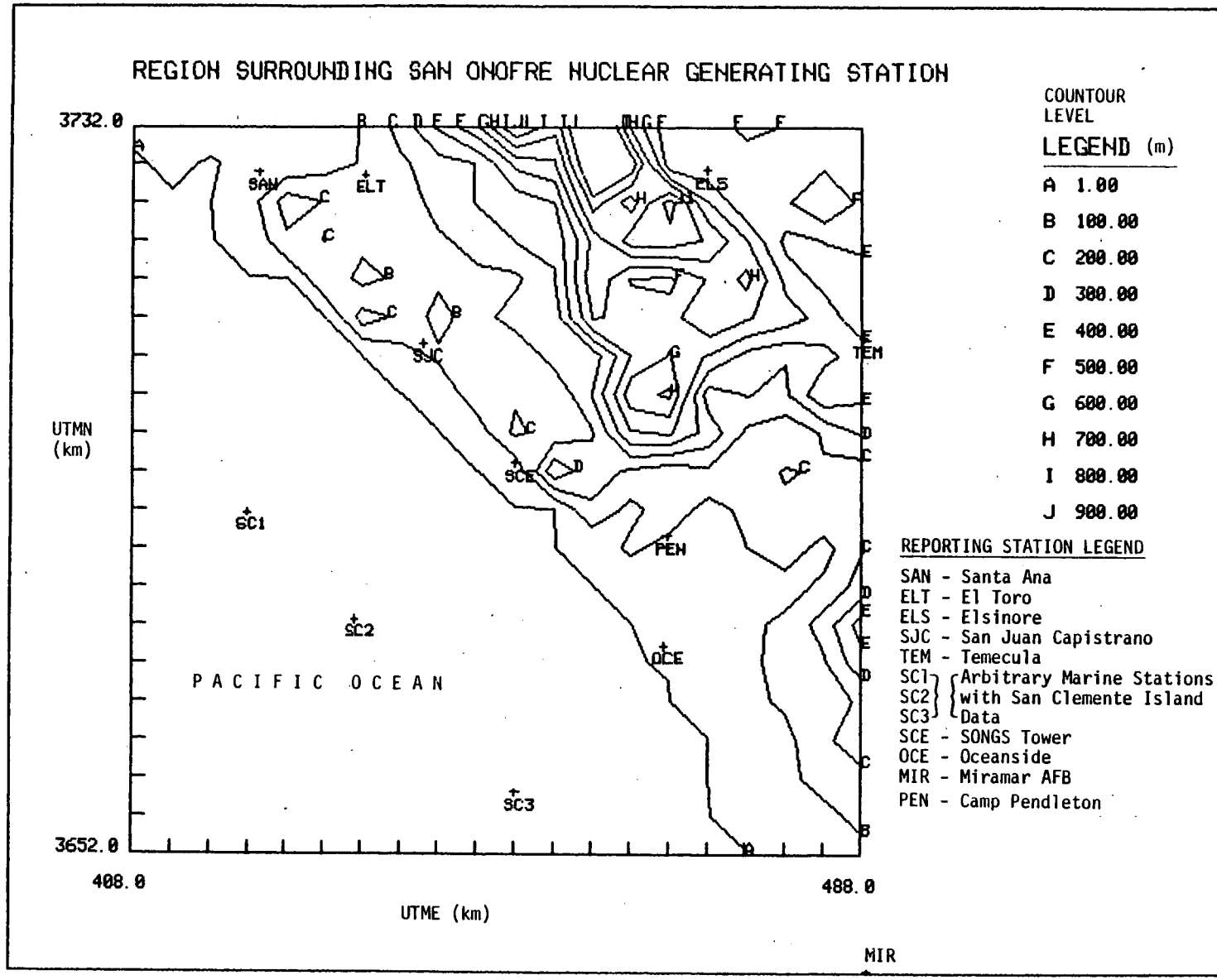

Figure 1-1. Region Surrounding San Onofre Nuclear Generating Station.

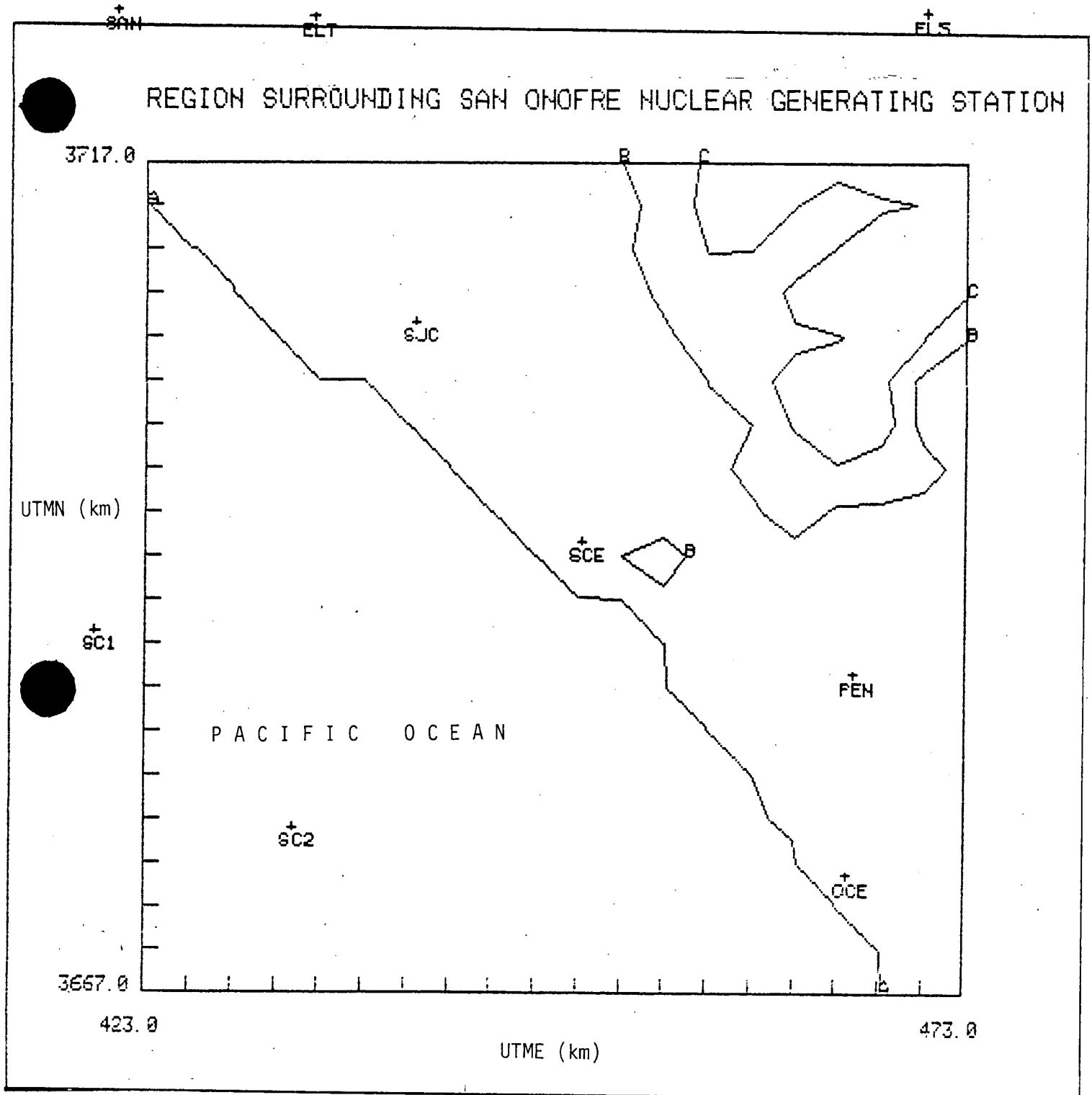

CONTOUR LEVEL LEGEND (m)

A	1.00
B	300.00
C	600.00
D	900.00

Figure 1-2. Physical Features of the Fifty Kilometer Square Study Area.

2.0 DESCRIPTION OF MODELS

2.1 MODEL FOR WIND AND STABILITY FIELDS

The development of the nonuniform wind fields for the SONGS study area was based on a version of the Dames & Moore proprietary computer model WNDSRF. Appendix A presents a technical description of this wind field development model. The version used in this study, WND2D2R, constructs a two-dimensional, surface (10-meter height) meteorological field on a uniform rectangular grid using meteorological data from scattered stations in the region of interest. The following steps comprise the basic modeling algorithms of the program:

1. Overlay the region of interest with a two-dimensional grid and specify terrain height and surface roughness values for each grid point.
2. Interpolate surface wind data from scattered meteorological measuring locations to grid points using local values of surface roughness and atmospheric stability.
3. Adjust wind vectors based on local diverting effects of the terrain.
4. Compute upslope or downslope wind components resulting from solar heating or cooling along sloping terrain.
5. Reduce anomalous divergence in the wind field using an interative procedure.

The techniques and functions used in this program are derived primarily from the analytic and semi-empirical models developed by Ryan (1977) using wind data collected at four research sites in the San Bernadino Mountains of southern California. Because of the complex terrain similarity between the San Bernadino area and the SONGS site, these models should be applicable to the SONGS study region.

Because of the availability of the meteorological data at SONGS and the application analysis for which these nonuniform meteorological

fields are needed, the basic WNDSRF program was modified for this study. The major modifications made to WNDSRF were as follows:

1. All surface roughness influences on the wind field were removed. Surface roughness effects on the atmospheric stability calculation were assumed to be contained within input stability class information.

2. The atmospheric mixing height influence on the wind field was removed. The calculated wind fields are relatively insensitive to the mixing height, so this change has only a very minor effect on the calculated wind fields.

3. Measured meteorological data are interpolated to grid points with a 1/R weighting factor in WND2D2R, where R is the distance to a given grid point. A $1/R^2$ weighting factor is used in WNDSRF. The 1/R weighting factor was judged to provide a smoother and more realistic variation of the calculated winds across the coastline.

4. The atmospheric stability field produced by WND2D2R is divided into three homogeneous regions: overwater, coastal, and inland. The stability class in each region is determined by input data from a single station in each region.

5. The meteorological data input from the measurement stations are restructured in WND2D2R to permit processing of non-sequential hours and grouping of data by meteorological monitoring station rather than by hour.

6. All calculated wind speeds in WND2D2R are normalized by the value of the input wind speed for the SONGS meteorological tower. This permits a variation of the wind speeds used in the dispersion calculation according to the real-time observed wind speed at the SONGS tower.

7. Various input control flags and parameters were changed in WND2D2R in order to accommodate the changes described above.

This modified wind and stability field development program was used to generate nonuniform wind and stability fields within a 50-km radius study area about the SONGS site. Representative nonuniform fields were selected for each meteorological category defined by observations at the SONGS tower. The selection of the representative fields is described in Section 3.4

2.2 MODEL FOR MIXING HEIGHT FIELDS AND POST-PROCESSING ADJUSTMENTS

The nonuniform mixing height field was developed subsequent to the wind and stability field generation. A separate post-processing program was developed to select and adjust the appropriate wind and stability fields and to generate the mixing height fields using the real-time onsite meteorological tower data at SONGS. A user's manual for this program, MXPROC, has been developed. This manual contains a overview of the computer program development, technical basis for program design, input and output requirements, and sample computer runs (Dames & Moore, 1982). The following presents, because of its importance in the development of the final nonuniform meteorological fields for use in the EARS, the technical information presented in this user's manual.

Meteorological Data Verification

The post-processor program MXPROC first performs data validity checks on the input meteorological parameters prior to performing any other operations. The printed output will identify 15-minute periods that have used default meteorological values because of the validity checks. This output identification will permit cognizance of default assignments prior to application in the transport and dispersion assessment as well as identify the possible need to initiate corrective maintenance of the meteorological data acquisition system.

Meteorological Index

The nonuniform wind and stability field records generated by the surface wind field program WND2D2R are used as input to MXPROC. A

total of 768 fields, based on the identification criteria, are possible (see Section 3.4). Each wind field record has been assigned a unique 6-digit meteorological index as follows:

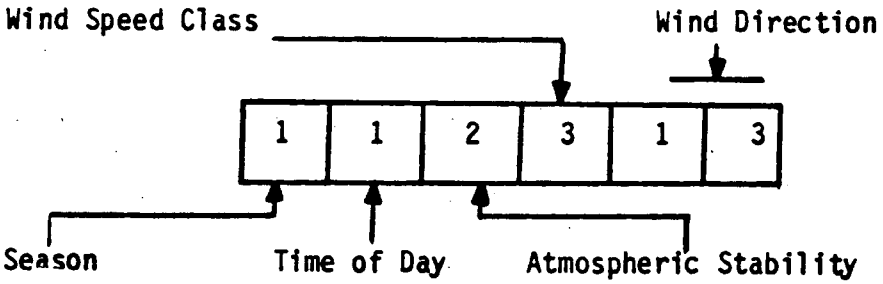

where:

Season	1 = winter /fall 2 = summer/spring
Time of Day	0 = night 1 = day
Atmospheric Stability:	1 = unstable (Pasquill Classes A-C) 2 = neutral (Pasquill Class D) 3 = stable (Pasquill Classes E-G)
Wind Speed Class:	1 = 0-4.0 mi/hr 2 = 4.1-8.0 mi/hr 3 = 8.1-12.0 mi/hr 4 = >12.0 mi/hr
Wind Direction:	1 through 16 sectors (NNE through N) from which the wind is blowing

Based on real-time 15-minute average meteorological conditions, MXPROC assigns the appropriate index to identify the particular nonuniform meteorological field appropriate for the present meteorological conditions. This index is then used to select and read the appropriate nonuniform wind and stability fields.

Wind Speed Adjustment

The nonuniform wind fields contain dimensionless horizontal wind components (normalized with respect to wind speed values at SONGS). These values must be scaled according to the real-time 15-minute average wind speed values measured at the bluff tower and converted to units of m/sec. In addition to performing this operation, MXPROC

restricts the resultant wind speed at each grid point to a value of no less than the SONGS minimum wind speed of 0.75 mi/hr (0.335 m/sec).

No adjustments are made to wind directions, because direction sectors are used as a basis for field selection and any adjustment based on SONGS observations alone would not be appropriate for all grid points.

Stability Adjustment

MXPROC converts the real-time differential-temperature data collected at the bluff tower to Pasquill stability class using the temperature-difference method recommended in NRC Regulatory Guide 1.23. The measured stability class at SONGS is used for the coastal zone. The difference between the real-time stability value measured at SONGS and the value of the stability field at the SONGS location contained in the stored nonuniform data file is then used to adjust the meteorological field stability values at both offshore and inland grid points. To provide a reasonable transition zone from offshore grid points to inland grid points, the following stability limitations are imposed at each grid point based on the real-time measurements at SONGS:

Measured Stability at SONGS	Allowed Stability at Offshore Grid Points	Allowed Stability at Inland Grid Points
A	C,D	A,B,C,D
B	C,D,E	A,B,C,D,E
C	C,D,E,F	A,B,C,D,E,F
D	C,D,E,F	A,B,C,D,E,F,G
E	C,D,E,F	B,C,D,E,F,G
F	C,D,E,F	C,D,E,F,G
G	D,E,F	D,E,F,G

Mixing Height Field

The mean seasonal morning and afternoon mixing height values, derived from the San Diego, California upper air station measurements

for the period 1960-64, were used to develop the nonuniform mixing height field surrounding the SONGS site (Holzworth, 1972). Initially MXPROC assigns the following uniform mixing height field according to the season of the year and the time of day:

Average Mixing Height	Winter	Spring	Summer	Autumn
Morning	534 m	851 m	538 m	578 m
Afternoon	1021 m	1085 m	566 m	834 m

Because the magnitude of the mixing height undergoes considerable diurnal and seasonal variations, changes in mixing height with stability is considered. Using the methodology developed for the Climatological Dispersion Model (CDM) by Busse and Zimmerman (1973), changes in the magnitude of the mixing height as a function of atmospheric stability at each grid point were assigned according to the following relationships:

Stability Class	Mixing Height Adjustment
A	1.5 x HA
B	HA
C	HA
D (day)	HA
D (night)	(HA + HM)/2
E	HM
F&G	HM

HA = average seasonal afternoon mixing height value.

HM = average seasonal morning mixing height value.

These general mixing height values near the coast can be dominated by the presence of an atmospheric coastal internal boundary layer. The conditions favorable to the development of an inland coastal internal boundary layer at the SONGS site are: (1) stable onshore gradient flow with the presence of a sea breeze on warm, clear, sunny days; (2) inland surface temperature warmer than the water surface temperature; and (3) neutral or unstable atmospheric conditions at some distance inland. Because most of these meteorological variables are not measured at the

bluff tower, the following criteria are used to identify the possible occurrence of coastal internal boundary layer development at SONGS:

1. Hours between sunrise and sunset;
2. The 15-minute average wind flow vector at the 10-meter level on the bluff tower is directed onshore between 143.5 and 263.5 degrees;
3. The 15-minute average wind speed at the 10-meter level on the bluff tower is equal to or exceeds 2 m/s;
4. The 15-minute average differential temperature at the bluff tower indicates the occurrence of a neutral or unstable atmospheric condition; and
5. The land-water temperature difference is greater than or equal to 1°C.

The magnitude of these criteria are arbitrary but are considered minimum values that are needed to have a coastal boundary layer develop.

Because the sea surface temperatures are not accessible to the Emergency Assessment and Response System (EARS) on a real-time basis, the following empirical equation derived by Ryan (1977) for the southern California area is used:

$$T_W = T_\phi + 2.2 \sin[0.986 (D+76) + 180]$$

and $T_\phi = 0.556 (64-\phi)$ for January through March

$= 0.972 (51.16-\phi)$ for April through December

where: T_W = Sea surface temperature (°C) as a function of the day of the year

T_ϕ = Approximate mean sea surface temperature (°C) as a function of latitude ϕ (ϕ = 33.37° for the SONGS site)

D = Julian day of the year

Two different approaches are used to estimate the coastal internal boundary layer growth. The first approach, in which the height of the internal boundary layer as a function of inland distance is determined empirically by the following power law relationship, is used only when

auto-convective temperature lapse rate conditions ($\Delta T \leq -3.42$ °C/100 m) are measured at the bluff tower:

$$L = C\, x^{1/2}$$

where: L = Height of the internal boundary layer (m)
x = Inland distance from the shoreline (m)
C = Empirical constant

This approach has been based on historical observations of hourly average differential temperature values in excess of the auto-convective lapse rate. The only explanation for this occurrence is the existance of a coastal internal boundary layer between the measurement levels (10-40 meters) on the tower. With an assumption that the height of the internal boundary layer is 40 meters at the bluff tower site during these conditions (located approximately 60 m inland from the shore), the empirical constant, C, is calculated to be 5.16.

In the second approach, the following semi-empirical equation developed by Raynor, et al. (1980) is used for predicting the height of the coastal internal boundary layer:

$$L = \frac{u^*}{u}\left[x\ \frac{\theta_W - \theta_L}{\Delta T/\Delta Z}\right]^{1/2}$$

where: L = Height of the internal boundary layer (m);
x = Inland distance from the shoreline (m);
u^* = Friction velocity over land (m/s);
u = Surface wind speed at 10-m level of the bluff tower (m/s);
θ_W = Surface potential temperature over water (K);
θ_L = Surface potential temperature over land (K); and
$\Delta T/\Delta Z$ = Temperature lapse rate between 10- and 40-m levels of the bluff tower (K/m).

The dimensionless friction velocity, u^*/u, over the land can be determined from the historical wind speed measurements at both the 10- and 40-m levels of the bluff tower by assuming the logarthmic relationship:

$$u = \frac{u^*}{k} \ln \frac{Z}{Z_0}$$

where: k = von Karman constant ($\simeq$0.4)

Z = Height of wind measurements above ground (m)

Z_0 = Surface roughness parameter (m)

A statistical analysis using 1976 hourly meteorological data collected from the bluff tower for all onshore, daytime, unstable and neutral atmospheric conditions, determined a value of 0.035 for u*/u at the 10-meter level for all neutral and unstable classifications.

The growth of the internal boundary layer as a function of the distance inland is assumed to cease when it intercepts the inland mixing height. During the presence of the internal boundary layer over land, the mixing heights at all grid points over the water are assumed to be zero. Assuming that the mixing height and internal boundary layer depth will follow topographic variations, the resulting mixing height field is further adjusted to include terrain elevation at each grid point.

3.0 METHODOLOGY

3.1 METEOROLOGICAL DATA

The sources of meteorological data in the 50-km square area surrounding the San Onofre Nuclear Generating Station (SONGS) were reviewed, in terms of availability and quality, for application in this study. The primary data were the observations taken at the SONGS bluff tower, which are referred to herein as the SONGS data. These data consisted of hourly-average values of wind speed and direction at three levels on the tower (10-m, 20-m, and 40-m), differential temperature from three sets of sensors (a primary and secondary set between 10 m and 40 m, and a third set between 20 feet and 120 feet), ambient temperature at the 10-m level, and horizontal wind direction standard deviation at the 10-m level.

The quality and quantity of meteorological observations at SONGS and the available meteorological observations from other sources for the year 1976 made this year the basic year of data for the analysis. This year of meteorological data was statistically compared to those of 1975 through 1979 to determine the representativeness of the 1976 year of data to the longer record at SONGS. This review, presented in Table 3-1, revealed the 1976 data period to be representative, in terms of stability, wind speed and wind direction, to that for the average of the five years. Because only the 10-m level wind speed and direction and the primary differential temperature measurements (secondary were used for invalid primary) were used in the following analysis, only these data were used in the comparison presented in Table 3-1.

Nine other meteorological stations were identified for use in this analysis. These data stations were selected based on their measurement location and data quality, as well as the data availability. These stations are described in Table 3-2 and their locations are shown in Figure 1-1.

Although only nine additional meteorological stations were used in the study, San Clemente Island was used at three separate locations

to represent the atmospheric conditions over the ocean. San Clemente Island is located approximately 100 km offshore from SONGS but was the only available data source that could be used to represent the offshore (ocean) atmospheric conditions. For the purpose of modeling, this station was placed at three separate locations parallel to the shoreline approximately 20 km offshore. The offshore distance of the three marine meteorological stations was chosen to produce realistic wind field modeling of the offshore convergence zone. This offshore convergence occurs whenever offshore (easterly or northeasterly) winds meet the generally westerly winds over the ocean. Typically, the resultant wind direction becomes roughly parallel to the coastline or stagnates in the offshore convergence zone.

The meteorological stations listed in Table 3-2 are of a variety of types. In addition to the SONGS data from the onsite tower, data consisting of 3-hourly observations were available from five National Weather Service stations, and data consisting of 1-hour average values of wind speed and direction were available from four air quality monitoring stations maintained by the South Coast Air Quality Management District (SCAQMD) and the San Diego Air Pollution Control District (SDAPCD). The modeling requires concurrent sequential observations throughout the entire field. Therefore, the basic meteorological data used in the nonuniform meteorological study were concurrent 3-hourly observations from 12 locations (nine different meteorological data stations) for the year 1976.

Because of the differences in the stability determination technique and the location and variability of available measurements, three stability regions were defined for the 50-km area about SONGS: inland, coastal and ocean regions. The meteorological stations selected to represent these three regions were:

- Coastal Region - SONGS differential temperature measurements were used to define Pasquill stability classes according to U.S. Nuclear Regulatory Commission Regulatory Guide 1.23 (USNRC, 1980).

- Inland Region - El Toro meteorological data were used to define stability classes according to the Pasquill-Turner technique (Turner, 1964).
- Ocean Region - San Clemente Island data were used to define the stability classes according to the Pasquill-Turner technique (Turner, 1964).

3.2 GENERATED METEOROLOGICAL FIELDS

The study area consisted of a square 50 km on each side centered approximately on the SONGS site. An initial study, described in Section 3.3, used a 40 x 40 grid of discrete points to represent the study area. One result of the initial work was the indication that an adequate resolution of detail in the computed wind fields was provided by a 20 x 20 grid of discrete points. The 20 x 20 grid was, therefore, used for the generated meteorological fields.

Wind speed and direction data were interpolated by the model, from the locations of the meteorological stations relative to grid points, using a 1/R weighting factor, where R is the distance from the station to any grid point. The radius of influence of each meteorological station was set equal to 15 grid squares, or a distance of 37.5 km for the 20 x 20 grid (grid points on the 20 x 20 grid were separated by 2.5 km). It was assumed that the measurement height was 10 m for each meteorological station.

Transmissivity indicates the fraction of radiation transmitted through the atmosphere and ranges from zero to one depending on the cloud cover. For sites without radiation data, Ryan (1977) recommends a transmissivity value of 0.45 for low to middle cloud cover of more than 0.5 and a value 0.90 for less cloud cover. A mean transmissivity to solar radiation of 0.65 was assumed in this study. This transmissivity figure is typical of the southern California region and was used in calculating the effects of insolation on steep terrain in the wind fields.

The defined 20 x 20 matrix, representing a 2,500 square kilometer area centered at SONGS, was used for the development of U- and

V-components of the wind field, atmospheric stability, and mixing height fields. The first three parameters were developed by the computer program WND2D2R, based on data from the nine meteorological measuring stations, and are subsequently adjusted by the post-processor program MXPROC using the real-time meteorological observations at SONGS. The mixing height fields are generated by the MXPROC program based on historical mixing height information adjusted by real-time SONGS measurements.

Figure 3-1 presents a typical wind field developed by WND2D2R. The meteorological data used in the generation of the wind field are given in Table 3-3. The actual output of WND2D2R used to develop Figure 3-1 was two files: one containing the U-component (east-west direction) of the wind with the second file containing the V-component (north-south direction) of the wind. All wind speeds have been normalized to that measured at the SONGS meteorological tower to enable adjustment of the values, during transport and dispersion application, to the real-time measurements from the SONGS meteorological tower. Because wind direction adjustments throughout the regional grid based on real-time SONGS tower measurements is not realistic nor appropriate due to the varying terrain, no direction adjustments are made to these data. Another reason not to impose a direction adjustment was the fact that the field selection criteria were based on wind direction sectors, not the actual direction readings.

The WND2D2R model also produced a nonuniform stability field for the study area. The stability field consisted of three regions: an ocean region, a coastal region, and an inland region. Within each region the stability was taken to be uniform and to equal the measured stability at a representative station. The three stability regions are shown in Figure 3-1.

Because different techniques of stability determination were used at the three regions, and because the real-time measured value at SONGS may be different than that used in the development of the stability field, adjustments to the stability field are made in the

post-processing program MXPROC. The selection criteria are based on three stability categories (stable, unstable, and neutral) while the actual real-time measurements at SONGS will be based on seven stability classes. The difference between the real-time measured stability at SONGS and the developed meteorological field value at the SONGS site is used to adjust the stability data field values at both offshore and inland grid points. The description of the MXPROC (Section 2.2) model provides more detail on this process.

The final point to be cognizant of in the review of the meteorological field development is the fact that meteorological measurement stations need not be located within the 20 x 20 matrix to affect the developed wind fields. The actual field used in the development of the 50 km by 50 km output grid extended beyond the limitations of the output area. As noted earlier, the radius of influence of each meteorological station is 37.5 km so that stations within this distance had an effect on the resultant wind fields. The Santa Ana, El Toro, Miramar, Elsinore, Temecula, and two of the arbitrary locations of San Clemente Island are examples of meteorological stations located outside the Figure 3-1 output grid that had an effect on the wind field development.

3.3 CATEGORIZATION OF METEOROLOGICAL FIELDS

The only real-time meteorological data routinely and automatically available to the SONGS Emergency Assessment and Response System (EARS) are those from the SONGS meteorological monitoring system. Therefore, to provide an operational system that does not require operator intervention, these real-time meteorological observations must be used to identify and develop nonuniform meteorological fields for use in the transport and dispersion assessments. The number of nonuniform meteorological fields that is needed to represent the regional transport and dispersion conditions is dependent on:

- The number of unique and significant meteorological regimes in terms of dispersion and transport conditions.

- The ability to distinguish between the various unique flow regimes given only the routine, real-time meteorological data available to the EARS.

Because of the limitation in both core storage and available computer time on the computer used for the EARS, the development and storage of a finite number of meteorological fields to represent the unique and significant flow regimes at SONGS was selected as the method of incorporating nonuniform meteorological analysis in the EARS. The initial study of the transport and dispersion conditions at SONGS revealed the need to define the total possible categories available, based on the important transport and dispersion parameters as measured on the SONGS tower, and to narrow these categories to a number that is reasonable to both review and handle on a routine basis. The first step, therefore, was to determine the type and number of categories that are both needed to represent the conditions at SONGS and are uniquely identifiable from the SONGS meteorological tower measurements.

The initial categorization was based on four wind speed classes, sixteen wind direction classes, three atmospheric stability classes, two diurnal classes, and four seasonal classes. This breakdown results in 1536 separate categories that cover the range of possible measurements at the SONGS site. The specific class limits used are shown in Table 3-4.

To distinguish between these categories in terms of importance, a frequency analysis was performed on the 1976 SONGS hourly data. The 1976 hourly data contained 8536 hours of simultaneously valid data for wind speed, wind direction, and stability. The distribution of these observations among the categories was very nonuniform. The most common types of flow were nighttime stable offshore winds and daytime unstable onshore winds. The most populous category was that for winter nighttime stable winds from the NNE, with wind speed between 8 mph and 12 mph, for which 245 observations occurred. For 654 of the 1536 categories (43 percent) there were no corresponding meteorological observations in the 1976 data. This analysis also revealed a similarity of

the frequency distributions for the spring and summer season and for the autumn and winter seasons.

A frequency analysis of the same categories was also performed on the 1977 SONGS meteorological data. The distribution for the 1977 data was very similar to that for the 1976 period. This result was taken as further evidence that the 1976 data period is representative of the SONGS site and, therefore, appropriate to characterize the site meteorology over a different and perhaps longer period of time.

To further determine the important categories at SONGS, a qualitative examination of the extent to which categories defined by the SONGS onsite data were representative of the observations obtained concurrently at the other meteorological stations was performed. Because the National Weather Service (NWS) station only routinely provides 3-hourly observations, this and subsequent analyses use 3-hourly data for all observation stations in the 1976 data period.

As a first step, the SONGS 1976 3-hourly data, concurrent with the hours for the 3-hourly NWS data, were used to identify periods when the following criteria were met. These criteria were chosen to characterize hours that would have the greatest likelihood of reflecting area-wide conditions.

1. Wind directions for the two surrounding hours were within ± 1 sector from the wind direction of the central hour.
2. Wind speeds for the two surrounding hours were within ± 4 mph from the wind speed of the central hour.
3. Stability conditions were in the same category for the 3-hour period (unstable, neutral, or stable).
4. Simultaneously valid measurements of wind speed, wind direction, and stability for the central hour.
5. No change in time of day (daytime, nighttime) or season during the 3-hourly observation period.

There were 1247 3-hour periods in the SONGS 1976 meteorological data that met all these criteria. This number is approximately 43 percent of the total of 2928 3-hour periods in 1976.

A frequency analysis was performed on the 1247 screened 3-hour periods, and categories with five or more occurrences were selected. There were 64 such categories. These 64 were reduced to 31 when the distinction between the seasons was eliminated. The number of periods in the 31 categories ranged from a minimum of five to a maximum of 167. Data for each hour in each of the 31 categories for each of the 10 meteorological stations listed in Table 3-2 were collected into files for use in the determination of the representativeness of the SONGS data for the region.

The first test performed on the 31 categories was an examination of the bivariate (wind speed and direction) frequency distributions for the other meteorological stations for each of the categories. This provided a direct test of the correlation between meteorological categories defined by the SONGS tower measurements and observations at the other stations in the area. The extent of the correlation between the SONGS data and that of the other stations varied considerably from one category to another, and also from one station to another within a category. Generally, the correlation ranged from fair to good, although very poor correlations were noted to occasionally occur, particularly for the stations most distant from the SONGS site. Some cases existed for which two or more distinct categories existing at another station could not be distinguished by data at SONGS.

To further test the selection criteria, selected hours of meteorological data chosen from the 31 categories were used in the WND2D2R model. The variability of the wind fields within a category with seasonal differences was in general small, and frequently smaller than the variability within the same season. Examination of a number of comparisons combined with the results of the frequency analysis led to the decision to divide the year into two "seasons" for the purpose of

subsequent study: Season 1 was defined as autumn and winter, and Season 2 was defined as spring and summer.

Sensitivity tests were performed to check the effect on the calculated wind fields of using two different interpolation weighting factors ($1/R$ and $1/R^2$), and different offshore distances at which the SC1, SC2, and SC3 stations (all using San Clemente Island data) were located. Subjective judgement concerning the realism of the calculated wind fields, as compared to normal meteorological conditions of southern California, produced the decision to use $1/R$ as the weighting factor for the interpolation and an offshore distance of approximately 20 km for the marine stations.

Finally, the 31 categories were used to test two separate methods of developing wind fields to represent categories. Initially, an average of all the hourly wind fields for a category was used to represent the wind field for a category. However, in many cases the average wind field was unlike any of the wind fields for the individual hours in the category. This situation could occur whenever one or more of the other meteorological stations did not have a good correlation with the other data stations in the category. Therefore, an alternative technique was used for the nonuniform wind field development wherein a single typical hour of meteorological data was chosen to represent the entire category. The criteria and methods for choosing the representative hour for a category are described in Section 3.4. This method of defining a meteorological field for a given category enabled the development of a flow regime based on current measured values rather than a non-existent average flow representative of average conditions.

The test modeling with WND2D2R was performed using a 40 x 40 grid to represent the study area. Examination of the resulting wind fields indicated adequate resolution of the wind direction and wind speed fields would be obtained using a 20 x 20 grid. Therefore, a 20 x 20 grid was used for all subsequent analysis.

The results of this initial analysis concerning the categorization of the meteorological fields are as follows:

- The categories for the identification of nonuniform meteorological fields using the routine SONGS meteorological tower data are distinguished by 2 classes based on seasons, 2 classes based on time of day, 3 stability classes, 4 wind speed classes, and 16 wind direction classes. This yields a total of 768 distinct categories or unique flow regimes.
- The nonuniform meteorological field representative of a particular category should be developed from a single hour of concurrent data from each station that is judged typical of the category.
- The three model marine meteorological stations should be located approximately 20 km offshore, paralleling the locations of the San Juan Capistrano, SONGS tower, and Oceanside meteorological stations.
- The wind field modeling should use a spatial weighting factor proportional to 1/R, where R is the distance between a meteorological station and any grid point of interest.
- A 20 x 20 grid matrix representing the study area adequately represents the details of the calculated wind fields.

3.4 DEVELOPMENT OF THE METEOROLOGICAL FIELDS

From the previous analysis 768 possible meteorological categories exist for the development of nonuniform meteorological fields. This number is based on the meteorological parameters routinely measured and available to the EARS and thought to be representative of possible different atmospheric flow regimes. Whether 768 distinct and unique atmospheric transport and dispersion conditions exist at SONGS was investigated through the analysis of the developed wind and stability field generated by the program WND2D2R. The following presents the

techniques and methods used to develop the final nonuniform meteorological fields.

In order to identify the 768 possible nonuniform meteorological fields, an index coding system was developed. A unique six-digit code was assigned, according to the scheme presented in Table 3-5, to each possible selection criteria. (Table 4-1 presents the matrix of 768 categories (possible fields) and their associated index.) For example, an observation at the SONGS tower at 10:00 a.m. on a morning in August showing a wind speed of 9.5 mph from the southwest and neutral atmospheric stability would be assigned the index of 212310. This index coding system was used throughout the following nonuniform meteorological field development both for the identification of particular fields and for the selection of meteorological fields by the post-processor program.

The 3-hourly SONGS meteorological data for 1976 were assigned the appropriate indices and these data, together with the concurrent observations from the other nine meteorological stations, were sorted by index. The number of hours assigned to an index varied from a minimum of zero for many indices of very low probability of occurrence (for example, most indices corresponding to daytime offshore stable flow), to a maximum of 158 hours assigned to index 103301, corresponding to the very common situation at SONGS of winter nighttime stable offshore flow. Of the 768 indices, 420 were observed one or more times in the SONGS 1976 3-hourly data. Table 3-6 presents the matrix of categories and the associated number of occurrence of each category in the SONGS 1976 3-hourly data.

The next task was the selection of a typical hour of concurrent meteorological data from all the stations for each index having more than one observation. For many indices with a small number of observations, the choice of a representative hour was unambiguous and straightforward. Other indices included many hours of observed data. The choice for such indices was sometimes difficult to make, and involved considerable subjective judgement. To ensure the selection of a

representative hour of concurrent meteorological data was performed correctly and appropriately, each index having five or more available hours in the 1976 period, of which there were 125 in number, was twice independently examined to select a representative hour. With a small number of exceptions, the person performing the second examination of an index was not the same person who performed the initial examination. In 52 cases the second examination produced a different representative hour than did the first examination. In these cases both of the chosen representative hours were analyzed, and the choice between the two was postponed until later in the analysis, subsequent to the development of the representative wind fields.

The basic criteria used to select the hour to represent an index with multiple observations were the following:

1. Delete hours for which data were missing at any of the important nearby stations of San Clemente Island, San Juan Capistrano, or Oceanside.
2. Delete hours for which the data at any of the important nearby stations clearly lie outside the dominating or prevailing characteristics for that station in the index.
3. Delete hours for which the indicated wind directions at the important nearby stations would lead to very large surface wind direction shifts in a short distance. (An example would be oppositely directed wind vectors at the SONGS tower and the San Juan Capistrano station.)
4. Delete hours for which data were missing from the more distant stations such as Santa Ana, El Toro, Miramar, etc.
5. If more than one hour survived Criteria 1 through 4, a choice was made among the remaining hours according to characteristics of the SONGS tower data. Criteria for selection in this step were:

a. Pick hours with wind directions nearer to the center of the meteorological sector.

b. Pick hours with valid ambient temperature data.

c. Pick hours with wind speeds nearer to the center of the defined wind speed classes.

Criterion 5 was used for only a very small number of indices with the largest populations. For most indices, the use of Criteria 1 through 3 was adequate to determine a representative hour.

For the second review of indices with more than five observations, very little emphasis was placed on Criterion 4. Even with one of the distant stations missing, the other stations could provide a meteorological field that better represents the index than an hour that had a complete set of meteorological data for all ten stations.

Nonuniform wind and stability fields were calculated, using the chosen representative hours, for each of the 420 indices having at least one observation. This resulted in 472 distinct sets of calculated wind and stability fields, because 52 of the indices had two representative hours selected. The calculated wind fields were printed out in graphic form to permit examination. An example of a wind field plot is presented in Figure 3-1. The data used to generate Figure 3-1 are given in Table 3-3.

The 472 separate wind field plots were each carefully examined in a cooperative effort between two Dames & Moore meteorologists and a meteorologist from Southern California Edison Company. This examination was designed to produce a final correspondence between calculated wind fields and indices. The final correspondence was not a one-to-one matching between each wind field and the index for which the representative hour was chosen. The calculated wind fields were subjectively judged by a number of criteria that could cause a particular wind field to be discarded, or to be used to represent more than a single index. The end product of this effort was to identify an appropriate meteorological field to be used for each index.

National Weather Service (NWS) daily weather maps were examined for the day associated with the data used as input to each of the wind fields. This review of the weather maps was made to identify and discard wind fields that were influenced by unusual or non-routine weather conditions such as hurricanes and heavy precipitation. This examination also revealed that reasonable wind flow characteristics of Santa Ana winds at the SONGS site were incorporated intrinsically by the selection of index values from measurements on the SONGS tower, so that no special provisions needed to be made to take Santa Ana conditions into account.

Another criterion used to judge the appropriateness of the calculated wind fields was the concept of temporal continuity of the wind field during operation of EARS. The system will use 15-minute average values of observed data at the SONGS tower to select nonuniform wind fields for the area. A small change in the measured data, for example, a 10-degree change in wind direction that might shift the direction from one meteorological sector to another, should not give rise to a very large change in the nonuniform wind field for the area. Rapid, large-scale changes in the general wind flow, although possible with frontal passages, were not of primary concern. Temporal and spatial changes in wind fields that were only one to two wind speed classes or wind direction sectors different from each other should show some continuity, if possible. Where possible, wind fields that were grossly different from a general pattern change in the neighboring index class wind field were discarded.

A criterion used to judge the applicability of a developed wind field was the shear and gradient of the surface winds. Surface wind flow patterns that were judged unlikely to exist, given the synoptic conditions displayed in the weather maps, were discarded if other wind fields could be used that presented a flow condition judged to be more realistic.

When appropriate and possible, a wind field calculated for one index was used to represent another index that had no associated wind

field either because there were no data for the index or because the associated wind field was rejected for reasons described above. Several criteria were used to guide such substitutions:

1. Temporal continuity - Where possible, the substituted wind field should be consistent with wind fields for neighboring indices (no abrupt change in flow patterns).

2. Wind direction class - No substitution involving a shift in wind direction class was allowed. That is, all substitution index fields must have the same last two digits.

3. Diurnal class - No substitution involving a shift from daytime to nighttime or vice versa was allowed.

4. Wind speed class - Substitutions were frequently made to adjacent wind speed classes. Multiple substitutions of this type could occur. This is an especially reasonable substitution as the final wind speeds are adjusted by the real-time measurements at SONGS.

5. Seasonal class - Substitution from one season to another was allowed.

6. Atmospheric stability class - Substitution from adjacent atmospheric stability classes was allowed.

As a result of the examination and selection procedure on the developed wind fields, 364 distinct wind fields were selected to represent 668 out of the 768 possible indices. A one-to-one correspondence of wind fields and stabilty fields was maintained throughout the analysis, so that each of the 668 indices represented also has associated with it an appropriate nonuniform stability field developed by the WND2D2R program. The remaining 100 indices, which primarily represent low-probability of occurrences at the SONGS site, could not be associated with an area-wide nonuniform wind field. For these 100 fields, a uniform wind flow pattern, based on the real-time measurement at the SONGS tower, is used.

3.5 INCORPORATION OF METEOROLOGICAL FIELDS INTO EARS

The wind and stability fields developed in Section 3.4 must be made available for use by the computer programs in EARS that perform the atmospheric transport and dispersion modeling. In addition, the nonuniform mixing height field must be developed for incorporation into the EARS modeling. The program MXPROC described in Section 2.2 performs the mixing height field development, wind and stability field selection, and post-processing adjustments to the fields. The use of this program with the developed wind fields and appropriate transport and dispersion models should complete the requirements for the release assessment.

One of the general operations of the MXPROC program is to select and read, from tape or disk storage of the fields, the appropriate nonuniform wind and stability fields given the real-time set of measured meteorological parameters from the SONGS tower. For those observations corresponding to an index for which no nonuniform meteorological field exists, MXPROC will generate uniform wind and stability fields based on the real-time SONGS meteorological measurements.

Another function performed by the MXPROC subroutine is to generate a nonuniform mixing height field to be used in the transport and dispersion model. The mixing height field is based on the seasonal average morning and afternoon mixing heights for the SONGS area as given by Holzworth (1972). The mixing height for each grid point is adjusted for the terrain and the stability class. MXPROC tests the meteorological data for conditions conducive to the formation of an onshore coastal internal boundary layer (CIBL). If the CIBL conditions are met, MXPROC limits the onshore mixing height to the calculated height of the CIBL for onshore distances for which the CIBL height is smaller than the mixing height calculated from the Holzworth values.

The details of the functioning of the MXPROC subroutine are presented in the MXPROC user's manual (Dames & Moore, 1982) and in Section 2.2.

TABLE 3-1

COMPARISON OF THE 1976 SONGS METEOROLOGICAL DATA*
WITH THE PERIOD 1975-1979

Wind Direction	1976 Percent Occurrence	1976 $\overline{u}$(m/s)	1975-1979 Percent Occurrence	1975-1979 $\overline{u}$(m/s)
NNE	21	3.8	22	3.5
NE	4	3.3	5	2.9
ENE	2	3.1	2	2.6
E	2	2.8	2	2.6
ESE	3	3.0	3	2.9
SE	6	3.4	7	3.3
SSE	7	3.7	7	3.7
S	7	3.6	6	3.4
SSW	5	3.3	5	3.1
SW	5	2.9	5	2.9
WSW	7	3.2	7	3.0
W	10	3.5	10	3.3
WNW	8	3.8	8	3.6
NW	4	3.4	4	3.3
NNW	3	1.3	3	2.5
N	5	2.3	4	2.6
Annual Average		3.5		3.2

STABILITY CLASS FREQUENCY

Pasquill-Turner Classification	1976 (Percent Frequency)	1975-1976 (Percent Frequency)
A	30.9	30.7
B	8.5	6.9
C	7.1	5.4
D	17.2	19.6
E	13.1	13.0
F	12.0	11.6
G	11.2	12.7

* 10-m level wind data and 10- to 40-m differential temperature data.

TABLE 3-2

METEOROLOGICAL DATA STATIONS USED IN THE SONGS NONUNIFORM WIND FIELD ANALYSIS

Station Name	Abbreviated Name[a]	Station Number	Station Type	Frequency of Available Data	Remarks
SONGS Bluff Tower	SCE	-	SONGS Onsite	Hourly	Primary data source; used to specify categories.
Santa Ana	SAN	93114	National Weather Service	3-Hourly	
El Toro MCAS	ELT	93101	U.S. Marine Corps Weather Station	3-Hourly	
Elsinore	ELS	-	SCAQMD[b]	Hourly	
San Juan Capistrano	SJC	-	SCAQMD	Hourly	
Temecula	TEM	-	SCAQMD	Hourly	
San Clemente Island	SC1 SC2 SC3	93117	Naval Weather Station	3-Hourly	Station characteristic of marine conditions; assigned to 3 model station locations 20 km offshore.
Camp Pendleton	PEN	03154	U.S. Marine Corps Weather Station	3-Hourly	Observations restricted to daylight hours; no data in 1976 after April.
Oceanside	OCE	-	SDAPCD[c]	Hourly	
Miramar NAS	MIR	93107	Naval Weather Station	3-Hourly	

[a]Corresponds to legend in Figure 1-1.
[b]SCAQMD = South Coast Air Quality Management District.
[c]SDAPCD = San Diego Air Pollution Control District.

TABLE 3-3

DATA USED TO GENERATE THE WIND FIELD SHOWN IN FIGURE 3-1[a]

	Station Code	Wind Direction	Wind Speed	Stability Class	Ambient Temperature
1	SCE	172.0	1.0	4	15.6
2	SC1	260.0	1.4	4	15.6
3	ELT	190.0	0.9	6	17.8
4	MIR	220.0	0.7	6	17.2
5	SAN	270.0	1.1	6	18.3
6	SC2	260.0	1.4	4	15.6
7	SC3	260.0	1.4	4	15.6
8	PEN	999.9[b]	999.9	999[b]	999.9
9	ELS	292.5	0.3	0[c]	0.0[c]
10	TEM	202.5	0.9	0	0.0
11	SJC	202.5	0.6	0	0.0
12	OCE	227.0	0.3	0	0.0

[a]Wind directions are in degrees from north, wind speeds are dimensionless multiples of the measured wind speed at the SCE station, and ambient temperatures are in °C.

[b]Invalid or missing data.

[c]Data not reported.

TABLE 3-4

CLASS LIMITS USED IN INITIAL CATEGORIZATION OF
SONGS 1976 ONSITE METEOROLOGICAL DATA

Wind Speed (MPH)	Wind Direction	Atmospheric Stability	Diurnal	Seasonal
0-4.0	NNE	Unstable	Day	Winter
4.1-8.0	NE	Neutral	Night	Spring
8.1-12.0	ENE	Stable		Summer
>12	E			Autumn
	ESE			
	SE			
	SSE			
	S			
	SSW			
	SW			
	WSW			
	W			
	WNW			
	NW			
	NNW			
	N			

TABLE 3-5

SIX-DIGIT INDEX ASSIGNMENT FOR EACH OF
768 METEOROLOGICAL CATEGORIES

Digit Number	Meteorological Variable	Coding
1	Season	1: Months September through February 2: Months March through August
2	Diurnal	0: Night 1: Day[a]
3	Atmospheric Stability	1: Unstable 2: Neutral 3: Stable
4	Wind Speed	1: WS <4 MPH 2: 4 MPH < WS ≤ 8 MPH 3: 8 MPH < WS ≤ 12 MPH 4: WS > 12 MPH
5,6	Wind Direction	01: NNE 02: NE 03: ENE 04: E 05: ESE 06: SE 07: SSE 08: S 09: SSW 10: SW 11: WSW 12: W 13: WNW 14: NW 15: NNW 16: N

[a]Day was defined as that part of each day during which the sun was above the horizon at an angle exceeding 15 degrees.

TABLE 3-6

DISTRIBUTION OF 3-HOURLY OBSERVATIONS BY METEOROLOGICAL CATEGORY
1976 METEOROLOGICAL DATA FROM THE SONGS TOWER

NIGHTTIME
SEASON - WINTER/AUTUMN

Wind Direction (Sectors)	Atmospheric Stability Classes											
	Unstable Wind Speed Class				Neutral Wind Speed Class				Stable Wind Speed Class			
	1	2	3	4	1	2	3	4	1	2	3	4
NNE	2	7	0	0	2	16	4	0	18	114	158	55
NE	0	1	0	0	1	1	0	1	17	39	15	14
ENE	0	2	0	0	0	1	0	2	6	12	2	5
E	0	1	0	1	4	3	0	3	9	7	0	2
ESE	0	2	1	3	1	4	3	0	5	13	0	0
SE	1	9	8	3	3	9	10	2	11	10	1	2
SSE	1	8	2	1	3	5	3	1	13	5	0	0
S	3	4	1	1	2	5	0	1	8	1	0	0
SSW	3	3	1	2	0	1	0	0	4	2	0	0
SW	1	0	0	3	2	2	0	0	2	1	0	0
WSW	1	3	3	0	2	0	1	1	2	0	0	0
W	2	1	0	0	3	1	1	0	3	1	0	0
WNW	4	6	0	0	1	0	0	0	4	2	0	0
NW	1	7	1	0	0	15	2	0	1	5	0	0
NNW	1	6	0	0	4	10	1	0	4	5	1	0
N	3	4	0	0	3	12	3	1	12	37	9	4

DAYTIME
SEASON - WINTER/AUTUMN

Wind Direction (Sectors)	Atmospheric Stability Classes											
	Unstable Wind Speed Class				Neutral Wind Speed Class				Stable Wind Speed Class			
	1	2	3	4	1	2	3	4	1	2	3	4
NNE	0	1	0	2	0	1	2	2	0	1	0	0
NE	0	0	2	1	0	1	0	0	0	0	0	0
ENE	0	0	0	2	0	0	0	1	0	0	0	0
E	0	0	0	1	0	0	0	0	0	1	0	0
ESE	0	0	0	3	0	0	0	0	0	0	0	0
SE	0	0	1	4	0	2	1	3	1	0	1	0
SSE	2	5	12	7	0	1	0	0	0	0	1	0
S	1	13	7	3	1	4	2	3	1	1	0	0
SSW	3	31	6	0	1	3	0	0	0	3	0	0
SW	3	27	3	0	0	3	0	0	0	0	1	0
WSW	1	32	16	1	0	2	0	0	4	1	1	0
W	1	53	31	2	1	7	1	0	2	9	2	0
WNW	1	19	37	8	1	5	3	0	1	8	4	0
NW	0	2	5	2	0	10	3	0	2	5	4	0
NNW	2	0	1	0	1	6	2	0	0	2	4	1
N	0	1	1	1	0	0	1	0	0	0	0	0

NIGHTTIME
SEASON - SUMMER/SPRING

Wind Direction (Sectors)	Atmospheric Stability Classes											
	Unstable Wind Speed Class				Neutral Wind Speed Class				Stable Wind Speed Class			
	1	2	3	4	1	2	3	4	1	2	3	4
NNE	1	3	2	0	4	20	4	0	11	89	77	19
NE	0	3	0	0	2	5	1	0	7	13	6	2
ENE	0	1	0	0	0	3	0	0	1	6	0	0
E	1	1	2	0	1	4	0	0	1	4	2	0
ESE	0	4	4	0	1	10	1	0	4	5	0	0
SE	3	14	14	3	2	37	10	0	2	9	0	1
SSE	0	22	20	8	4	17	3	0	2	2	0	0
S	0	16	4	2	1	14	3	0	2	0	0	0
SSW	1	6	2	1	2	7	1	0	1	1	0	0
SW	2	11	3	1	1	2	0	0	0	0	0	0
WSW	3	7	2	1	3	4	0	0	0	1	0	0
W	5	12	1	0	1	5	2	0	0	0	0	0
WNW	2	18	3	1	3	5	0	2	0	1	0	1
NW	0	15	15	1	2	5	1	3	0	1	2	0
NNW	2	4	2	0	0	10	3	0	0	2	1	0
N	3	4	1	0	8	11	1	0	0	12	10	1

DAYTIME
SEASON - SUMMER/SPRING

Wind Direction (Sectors)	Atmospheric Stability Classes											
	Unstable Wind Speed Class				Neutral Wind Speed Class				Stable Wind Speed Class			
	1	2	3	4	1	2	3	4	1	2	3	4
NNE	0	3	1	0	1	2	0	0	0	0	0	0
NE	0	1	0	0	0	1	0	0	0	0	0	0
ENE	0	0	0	0	0	0	0	0	0	0	0	0
E	0	2	0	0	0	0	0	0	0	0	0	0
ESE	0	1	0	0	0	1	0	0	0	0	0	0
SE	0	3	6	0	0	1	0	0	0	0	0	0
SSE	1	10	10	15	0	4	0	1	1	1	1	0
S	0	26	34	11	0	2	0	0	0	1	0	0
SSW	0	40	28	12	0	2	0	1	0	0	0	0
SW	2	50	13	1	0	0	2	0	2	3	0	0
WSW	2	53	37	4	0	1	1	0	1	0	0	0
W	0	58	89	6	1	1	1	0	2	1	1	0
WNW	0	16	38	16	0	5	1	2	0	3	5	0
NW	1	2	5	0	0	2	1	0	0	1	1	0
NNW	0	3	0	1	0	0	0	0	0	0	0	0
N	0	1	0	0	0	1	0	0	0	0	0	0

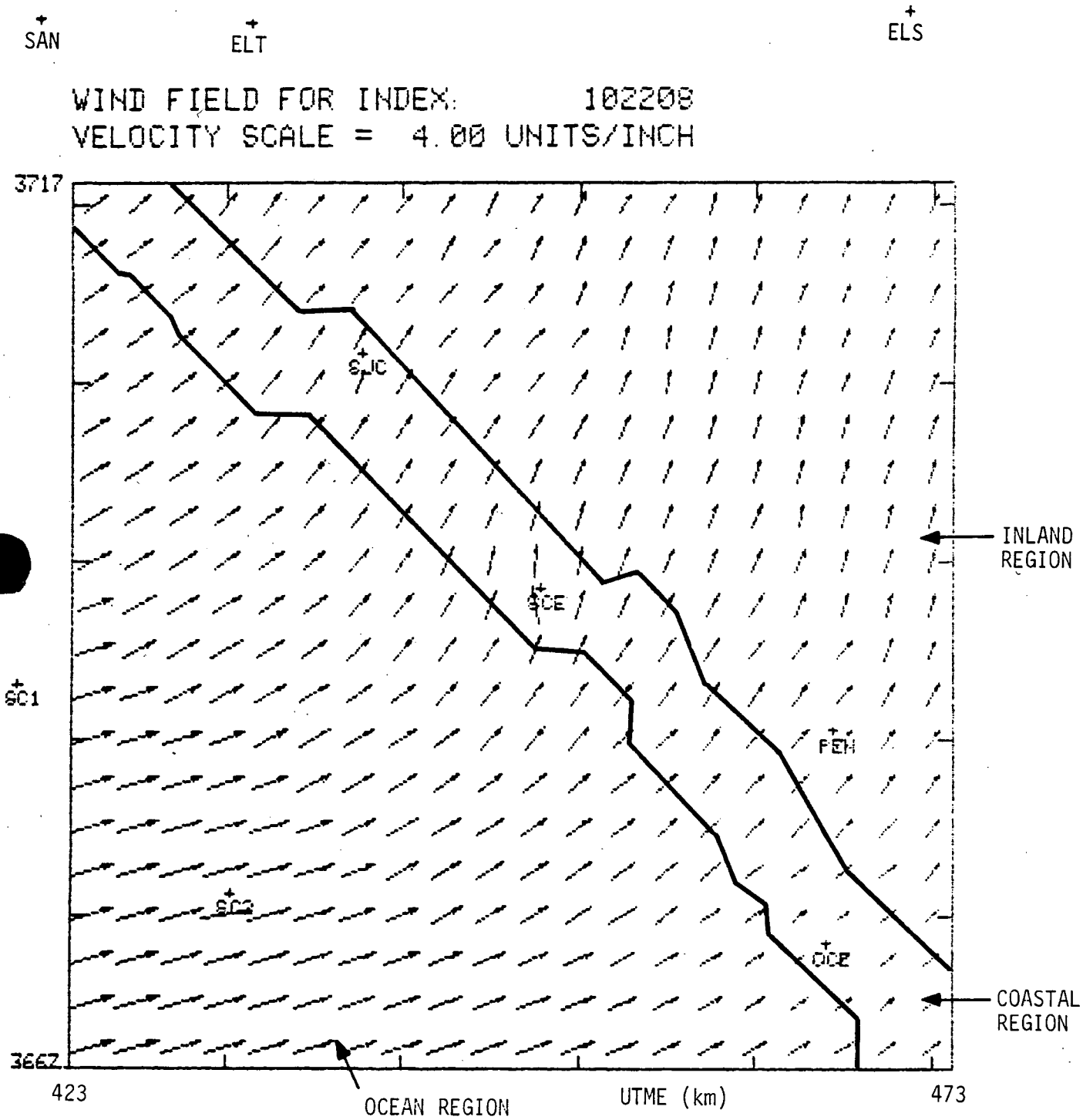

Figure 3-1. Study Area Covered by Modeling of Meteorological Fields. The Arrows Show A Typical Windfield Calculated on the 20 x 20 Grid. Also Shown are the 3 Regions Used to Describe the Atmospheric Stability Field.

4.0 RESULTS

Plots of each of the 364 nonuniform wind fields developed in this study for use in the SONGS EARS are presented in Appendix B. The associated stability fields, which consist of uniform stabilities within each of the three regions shown in Figure 3-1, are not presented in this document. A magnetic tape containing all the nonuniform wind and stability fields was supplied and provides the basis for input to the MXPROC post-processor program. The magnitude of the wind vector in all of the wind fields, on both the magnetic tape and the plots, is scaled to a value of unity at the location of the SONGS tower.

The wind field assigned to any set of meteorological conditions observed at the SONGS tower can be obtained by the following process:

1. Locate the matrix position corresponding to the SONGS tower meteorological conditions in Table 4-1. The top matrix element in the table presents the appropriate index for the meteorological conditions of the matrix position while the bottom matrix element is the corresponding record number of the wind and stability field as stored on the magnetic tape. A record number of 999 indicates that a uniform field is assigned.

2. Refer to Table 4-2 to find the index corresponding to the record number found in Step 1. The index in Table 4-2 assigned to the particular record number does not necessarily agree with the index associated with the matrix position in Table 4-1 because of the selection process (see Section 3.4). Table 4-2 index assignments reflect the selection of representative meteorological fields for each matrix position.

3. Find the wind field in Appendix B labeled by the index found in Step 2. The wind fields in Appendix B are ordered by index.

Figure 4-1 is an example of a typical nonuniform wind field for nighttime stable offshore flow, which is the type of flow most frequently encountered at the SONGS site. Note the offshore convergence of the wind vectors, which is a typical and important aspect of this type of flow. Figure 1-2 should be used to identify the location of regional physical features in Figures 4-1 and 4-2.

Figure 4-2 is an example of a typical nonuniform wind field for daytime unstable onshore flow, which is the second most frequently occurring flow type encountered at the SONGS site. Note the strong influence of terrain on the wind vectors in the upper right hand quadrant of this figure.

As an example of the determination of the wind assignment for a particular set of meteorological conditions, the following is offered:

Date:	April 30, 1982
Time:	4 p.m.
Wind Speed:	2 mi/hr
Wind Direction:	160 degree
Ambient Air Temperature:	25°C
Delta-temperature (40-10 m):	1.5°C/30m (Pasquill Class G)

The meteorological index code for this measured meteorological condition is 213107. From Table 4-1 the record number for this meteorological condition is 356. The assigned meteorological field for this observation has the index of 213207 (Table 4-2). This assigned index indicates the next higher wind speed class was assigned to the matrix position. The display of the wind field for this meteorological category can be obtained by selecting the wind field from Appendix B associated with index 213207.

TABLE 4-1

TABLE OF RECORD NUMBER BY METEOROLOGICAL CONDITIONS (INDEX)
PART A: NIGHT HOURS FOR MONTHS SEPTEMBER THROUGH FEBRUARY (AUTUMN/WINTER)

Wind Direction (Sector)	ATMOSPHERIC STABILITY CLASS											
	Unstable				Neutral				Stable			
	Wind Speed Class				Wind Speed Class				Wind Speed Class			
	1	2	3	4	1	2	3	4	1	2	3	4
NNE	101101 7	101201 7	101301 7	101401 7	102101 46	102201 46	102301 58	102401 58	103101 75	103201 90	103301 104	103401 110
NE	101102 8	101202 8	101302 8	101402 999	102102 35	102202 35	102302 67	102402 67	103102 76	103202 91	103302 105	103402 111
ENE	101103 9	101203 9	101303 9	101403 9	102103 47	102203 47	102303 68	102403 68	103103 77	103203 92	103303 106	103403 112
E	101104 10	101204 10	101304 10	101404 10	102104 48	102204 48	102304 69	102404 69	103104 78	103204 93	103304 93	103404 113
ESE	101105 11	101205 11	101305 22	101405 29	102105 36	102205 59	102305 59	102405 59	103105 79	103205 94	103305 94	103405 94
SE	101106 1	101206 12	101306 23	101406 30	102106 37	102206 49	102306 60	102406 70	103106 80	103206 95	103306 107	103406 114
SSE	101107 13	101207 13	101307 24	101407 31	102107 38	102207 50	102307 61	102407 71	103107 81	103207 96	103307 96	103407 96
S	101108 2	101208 14	101308 25	101408 32	102108 39	102208 51	102308 72	102408 72	103108 82	103208 97	103308 97	103408 97
SSW	101109 3	101209 15	101309 26	101409 33	102109 52	102209 52	102309 999	102409 999	103109 83	103209 98	103309 98	103409 98
SW	101110 4	101210 34	101310 34	101410 34	102110 40	102210 53	102310 53	102410 53	103110 84	103210 99	103310 99	103410 99
WSW	101111 16	101211 16	101311 27	101411 27	102111 41	102211 41	102311 62	102411 73	103111 85	103211 62	103311 62	103411 73
W	101112 17	101212 17	101312 17	101412 17	102112 42	102212 54	102312 63	102412 63	103112 86	103212 54	103312 63	103412 63
WNW	101113 5	101213 18	101313 18	101413 18	102113 43	102213 43	102313 999	102413 999	103113 87	103213 100	103313 100	103413 999
NW	101114 19	101214 19	101314 28	101414 28	102114 55	102214 55	102314 64	102414 64	103114 101	103214 101	103314 101	103414 101
NNW	101115 20	101215 20	101315 20	101415 20	102115 44	102215 56	102315 65	102415 65	103115 88	103215 102	103315 108	103415 108
N	101116 6	101216 21	101316 21	101416 21	102116 45	102216 57	102316 66	102416 74	103116 89	103216 103	103316 109	103416 115

PART B: DAY HOURS FOR MONTHS SEPTEMBER THROUGH FEBRUARY (AUTUMN/WINTER)

Wind Direction (Sector)	ATMOSPHERIC STABILITY CLASS											
	Unstable				Neutral				Stable			
	Wind Speed Class				Wind Speed Class				Wind Speed Class			
	1	2	3	4	1	2	3	4	1	2	3	4
NNE	111101	111201	111301	111401	112101	112201	112301	112401	113101	113201	113301	113401
	149	149	135	135	149	149	160	165	174	174	174	999
NE	111102	111202	111302	111402	112102	112202	112302	112402	113102	113202	113302	113402
	124	124	124	136	150	150	999	999	999	999	999	999
ENE	111103	111203	111303	111403	112103	112203	112303	112403	113103	113203	113303	113403
	137	137	137	137	166	166	166	166	999	999	999	999
E	111104	111204	111304	111404	112104	112204	112304	112404	113104	113204	113304	113404
	138	138	138	138	999	999	999	999	175	175	999	999
ESE	111105	111205	111305	111405	112105	112205	112305	112405	113105	113205	113305	113405
	302	302	139	139	999	999	999	999	999	999	999	999
SE	111106	111206	111306	111406	112106	112206	112306	112406	113106	113206	113306	113406
	125	125	125	140	151	151	167	167	183	183	183	183
SSE	111107	111207	111307	111407	112107	112207	112307	112407	113107	113207	113307	113407
	117	117	126	141	152	152	999	999	356	356	362	999
S	111108	111208	111308	111408	112108	112208	112308	112408	113108	113208	113308	113408
	118	118	127	142	148	153	161	168	169	176	176	176
SSW	111109	111209	111309	111409	112109	112209	112309	112409	113109	113209	113309	113409
	116	119	128	128	154	154	154	154	177	177	177	177
SW	111110	111210	111310	111410	112110	112210	112310	112410	113110	113210	113310	113410
	120	120	120	120	999	999	999	999	184	184	184	184
WSW	111111	111211	111311	111411	112111	112211	112311	112411	113111	113211	113311	113411
	121	121	129	143	155	155	155	155	170	178	178	178
W	111112	111212	111312	111412	112112	112212	112312	112412	113112	113212	113312	113412
	122	122	130	144	156	156	999	999	171	179	185	185
WNW	111113	111213	111313	111413	112113	112213	112313	112413	113113	113213	113313	113413
	123	123	131	145	157	157	999	999	172	180	186	186
NW	111114	111214	111314	111414	112114	112214	112314	112414	113114	113214	113314	113414
	132	132	132	146	158	158	162	162	173	181	187	187
NNW	111115	111215	111315	111415	112115	112215	112315	112415	113115	113215	113315	113415
	133	133	133	133	159	159	163	163	182	182	188	189
N	111116	111216	111316	111416	112116	112216	112316	112416	113116	113216	113316	113416
	999	999	134	147	999	999	164	164	999	999	999	999

PART C: NIGHT HOURS FOR MONTHS MARCH THROUGH AUGUST (SPRING/SUMMER)

Wind Direction (Sector)	ATMOSPHERIC STABILITY CLASS											
	Unstable				Neutral				Stable			
	Wind Speed Class				Wind Speed Class				Wind Speed Class			
	1	2	3	4	1	2	3	4	1	2	3	4
NNE	201101	201201	201301	201401	202101	202201	202301	202401	203101	203201	203301	203401
	190	198	214	214	233	242	242	242	274	274	286	290
NE	201102	201202	201302	201402	202102	202202	202302	202402	203102	203202	203302	203402
	199	199	199	999	234	243	258	258	269	269	287	291
ENE	201103	201203	201303	201403	202103	202203	202303	202403	203103	203203	203303	203403
	200	200	200	999	244	244	244	68	275	275	275	275
E	201104	201204	201304	201404	202104	202204	202304	202404	203104	203204	203304	203404
	191	201	215	215	245	245	245	245	276	276	276	276
ESE	201105	201205	201305	201405	202105	202205	202305	202405	203105	203205	203305	203405
	202	202	216	216	246	246	259	259	277	277	277	999
SE	201106	201206	201306	201406	202106	202206	202306	202406	203106	203206	203306	203406
	192	203	217	228	235	247	260	70	270	278	292	292
SSE	201107	201207	201307	201407	202107	202207	202307	202407	203107	203207	203307	203407
	204	204	218	229	236	248	261	261	271	279	279	999
S	201108	201208	201308	201408	202108	202208	202308	202408	203108	203208	203308	203408
	205	205	219	230	249	249	262	262	272	249	262	262
SSW	201109	201209	201309	201409	202109	202209	202309	202409	203109	203209	203309	203409
	193	206	220	231	237	250	250	250	273	280	280	280
SW	201110	201210	201310	201410	202110	202210	202310	202410	203110	203210	203310	203410
	194	207	221	221	251	251	251	251	251	251	251	251
WSW	201111	201211	201311	201411	202111	202211	202311	202411	203111	203211	203311	203411
	195	208	222	222	238	252	252	73	238	281	281	281
W	201112	201212	201312	201412	202112	202212	202312	202412	203112	203212	203312	203412
	196	209	223	223	239	253	263	263	239	253	263	263
WNW	201113	201213	201313	201413	202113	202213	202313	202413	203113	203213	203313	203413
	197	210	224	224	254	254	254	267	282	282	293	293
NW	201114	201214	201314	201414	202114	202214	202314	202414	203114	203214	203314	203414
	211	211	225	232	240	255	264	268	283	283	288	288
NNW	201115	201215	201315	201415	202115	202215	202315	202415	203115	203215	203315	203415
	212	212	226	226	256	256	265	265	284	284	289	289
N	201116	201216	201316	201416	202116	202216	202316	202416	203116	203216	203316	203416
	213	213	227	227	241	257	266	999	285	285	294	294

PART D: DAY HOURS FOR MONTHS MARCH THROUGH AUGUST (SPRING/SUMMER)

Wind Direction (Sector)	ATMOSPHERIC STABILITY CLASS											
	Unstable				Neutral				Stable			
	Wind Speed Class				Wind Speed Class				Wind Speed Class			
	1	2	3	4	1	2	3	4	1	2	3	4
NNE	211101	211201	211301	211401	212101	212201	212301	212401	213101	213201	213301	213401
	299	299	314	314	332	334	160	165	999	999	999	999
NE	211102	211202	211302	211402	212102	212202	212302	212402	213102	213202	213302	213402
	300	300	300	136	335	335	335	999	999	999	999	999
ENE	211103	211203	211303	211403	212103	212203	212303	212403	213103	213203	213303	213403
	999	999	137	137	999	999	166	166	999	999	999	999
E	211104	211204	211304	211404	212104	212204	212304	212404	213104	213204	213304	213404
	301	301	138	138	999	999	999	999	175	175	999	999
ESE	211105	211205	211305	211405	212105	212205	212305	212405	213105	213205	213305	213405
	302	302	302	139	336	336	336	999	999	999	999	999
SE	211106	211206	211306	211406	212106	212206	212306	212406	213106	213206	213306	213406
	303	303	315	315	337	337	337	167	999	183	183	999
SSE	211107	211207	211307	211407	212107	212207	212307	212407	213107	213207	213307	213407
	295	304	316	324	338	338	350	350	356	356	362	999
S	211108	211208	211308	211408	212108	212208	212308	212408	213108	213208	213308	213408
	305	305	317	325	339	339	339	168	357	357	999	999
SSW	211109	211209	211309	211409	212109	212209	212309	212409	213109	213209	213309	213409
	306	306	318	326	340	340	351	351	177	177	177	177
SW	211110	211210	211310	211410	212110	212210	212310	212410	213110	213210	213310	213410
	296	307	319	327	999	345	345	345	353	358	358	358
WSW	211111	211211	211311	211411	212111	212211	212311	212411	213111	213211	213311	213411
	297	308	320	328	341	341	346	346	354	178	999	999
W	211112	211212	211312	211412	212112	212212	212312	212412	213112	213212	213312	213412
	309	309	321	329	333	333	347	347	355	359	363	999
WNW	211113	211213	211313	211413	212113	212213	212313	212413	213113	213213	213313	213413
	310	310	322	330	342	342	348	352	360	360	364	364
NW	211114	211214	211314	211414	212114	212214	212314	212414	213114	213214	213314	213414
	298	311	323	323	343	343	349	349	361	361	361	999
NNW	211115	211215	211315	211415	212115	212215	212315	212415	213115	213215	213315	213415
	312	312	331	331	999	159	163	999	999	999	188	999
N	211116	211216	211316	211416	212116	212216	212316	212416	212116	213216	213316	213416
	313	313	147	147	344	344	999	999	999	999	999	999

TABLE 4-1 (Continued)

[a]Day hours correspond to those for which the sun's angle above the horizon exceeds 15 degrees

[b]Wind speed (WS) classes:
1: WS ≤4 MPH
2: 4 MPH < WS ≤ 8 MPH
3: 8 MPH < WS ≤ 12 MPH
4: WS > 12 MPH

[c]Matrix elements consist of the index associated with the meteorological conditions of the matrix position followed by the record number of the wind and stability field as stored on the magnetic tape.

[d]A record number of 999 indicates a uniform field is to be assigned.

TABLE 4-2

TABLE OF INDICES BY TAPE RECORD NUMBER

Rec. No.	Index	Rec. No.	Index	Rec. No.	Index
1	101106	41	102111	81	103107
2	101108	42	102112	82	103108
3	101109	43	102113	83	103109
4	101110	44	102115	84	103110
5	101113	45	102116	85	103111
6	101116	46	102201	86	103112
7	101201	47	102203	87	103113
8	101202	48	102204	88	103115
9	101203	49	102206	89	103116
10	101204	50	102207	90	103201
11	101205	51	102208	91	103202
12	101206	52	102209	92	103203
13	101207	53	102210	93	103204
14	101208	54	102212	94	103205
15	101209	55	102214	95	103206
16	101211	56	102215	96	103207
17	101212	57	102216	97	103208
18	101213	58	102301	98	103209
19	101214	59	102305	99	103210
20	101215	60	102306	100	103213
21	101216	61	102307	101	103214
22	101305	62	102311	102	103215
23	101306	63	102312	103	103216
24	101307	64	102314	104	103301
25	101308	65	102315	105	103302
26	101309	66	102316	106	103303
27	101311	67	102402	107	103306
28	101314	68	102403	108	103315
29	101405	69	102404	109	103316
30	101406	70	102406	110	103401
31	101407	71	102407	111	103402
32	101408	72	102408	112	103403
33	101409	73	102411	113	103404
34	101410	74	102416	114	103406
35	102102	75	103101	115	103416
36	102105	76	103102	116	111109
37	102106	77	103103	117	111207
38	102107	78	103104	118	111208
39	102108	79	103105	119	111209
40	102110	80	103106	120	111210

TABLE 4-2 (Continued)

Rec. No.	Index	Rec. No.	Index	Rec. No.	Index
121	111211	161	112308	201	201204
122	111212	162	112314	202	201205
123	111213	163	112315	203	201206
124	111302	164	112316	204	201207
125	111306	165	112401	205	201208
126	111307	166	112403	206	201209
127	111308	167	112406	207	201210
128	111309	168	112408	208	201211
129	111311	169	113108	209	201212
130	111312	170	113111	210	201213
131	111313	171	113112	211	201214
132	111314	172	113113	212	201215
133	111315	173	113114	213	201216
134	111316	174	113201	214	201301
135	111401	175	113204	215	201304
136	111402	176	113208	216	201305
137	111403	177	113209	217	201306
138	111404	178	113211	218	201307
139	111405	179	113212	219	201308
140	111406	180	113213	220	201309
141	111407	181	113214	221	201310
142	111408	182	113215	222	201311
143	111411	183	113306	223	210312
144	111412	184	113310	224	201313
145	111413	185	113312	225	201314
146	111414	186	113313	226	201315
147	111416	187	113314	227	201316
148	112108	188	113315	228	201406
149	112201	189	113415	229	201407
150	112202	190	201101	230	201408
151	112206	191	201104	231	201409
152	112207	192	201106	232	201414
153	112208	193	201109	233	202101
154	112209	194	201110	234	202102
155	112211	195	201111	235	202106
156	112212	196	201112	236	202107
157	112213	197	201113	237	202109
158	112214	198	201201	238	202111
159	112215	199	201202	239	202112
160	112301	200	201203	240	202114

TABLE 4-2 (Continued)

Rec. No.	Index	Rec. No.	Index	Rec. No.	Index
241	202116	281	203211	321	211312
242	202201	282	203213	322	211313
243	202202	283	203214	323	211314
244	202203	284	203215	324	211407
245	202204	285	203216	325	211408
246	202205	286	203301	326	211409
247	202206	287	203302	327	211410
248	202207	288	203314	328	211411
249	202208	289	203315	329	211412
250	202209	290	203401	330	211413
251	202210	291	203402	331	211415
252	202211	292	203406	332	212101
253	202212	293	203413	333	212112
254	202213	294	203416	334	212201
255	202214	295	211107	335	212202
256	202215	296	211110	336	212205
257	202216	297	211111	337	212206
258	202302	298	211114	338	212207
259	202305	299	211201	339	212208
260	202306	300	211202	340	212209
261	202307	301	211204	341	212211
262	202308	302	211205	342	212213
263	202312	303	211206	343	212214
264	202314	304	211207	344	212216
265	202315	305	211208	345	212310
266	202316	306	211209	346	212311
267	202413	307	211210	347	212312
268	202414	308	211211	348	212313
269	203102	309	211212	349	212314
270	203106	310	211213	350	212407
271	203107	311	211214	351	212409
272	203108	312	211215	352	212413
273	203109	313	211216	353	213110
274	203201	314	211301	354	213111
275	203203	315	211306	355	213112
276	203204	316	211307	356	213207
277	203205	317	211308	357	213208
278	203206	318	211309	358	213210
279	203207	319	211310	359	213212
280	203209	320	211311	360	213213

TABLE 4-2 (Continued)

Rec. No.	Index
361	213214
362	213307
363	213312
364	213313

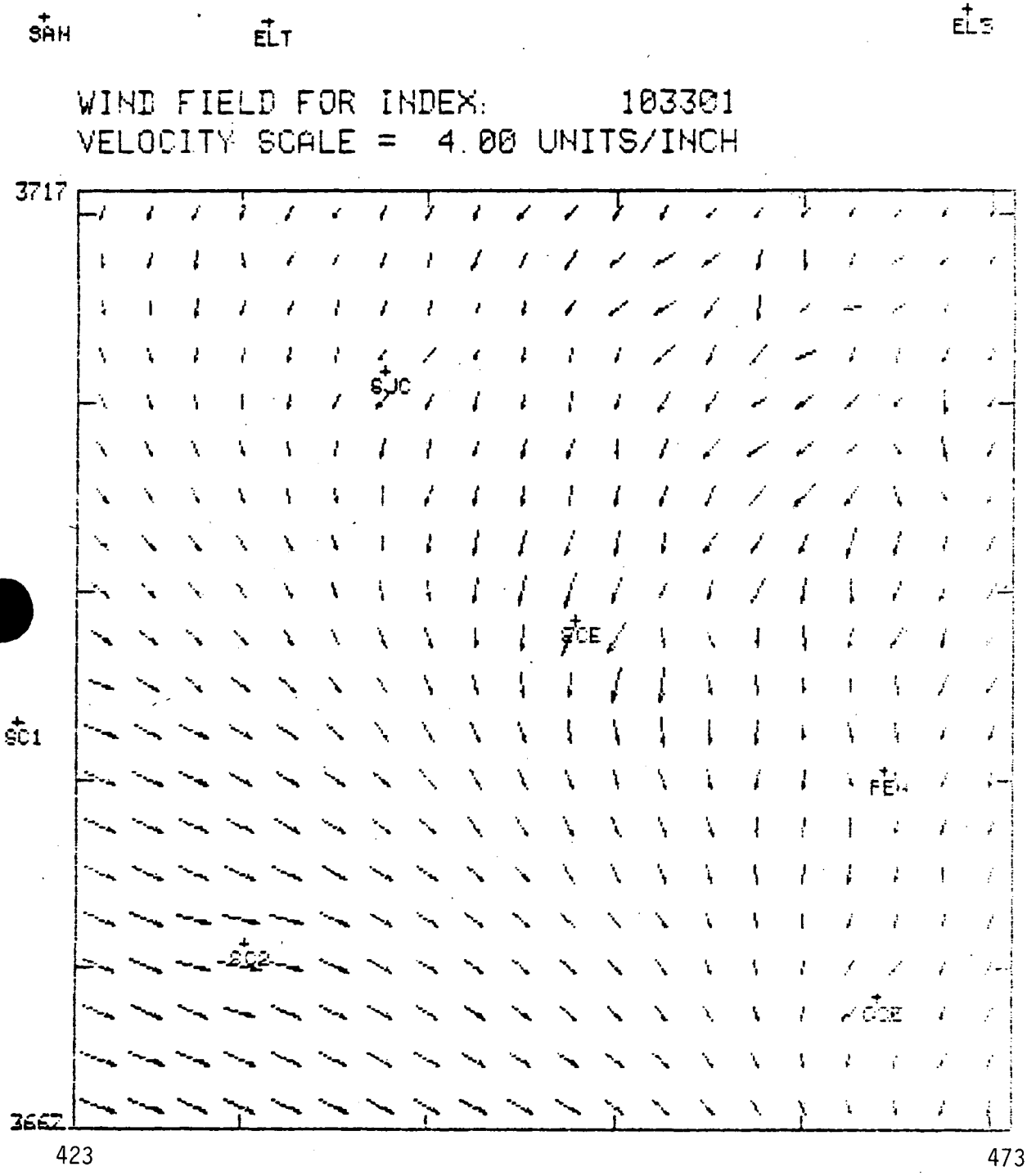

Figure 4-1. A Typical Wind Field Plot for Nighttime Stable Offshore Flow.

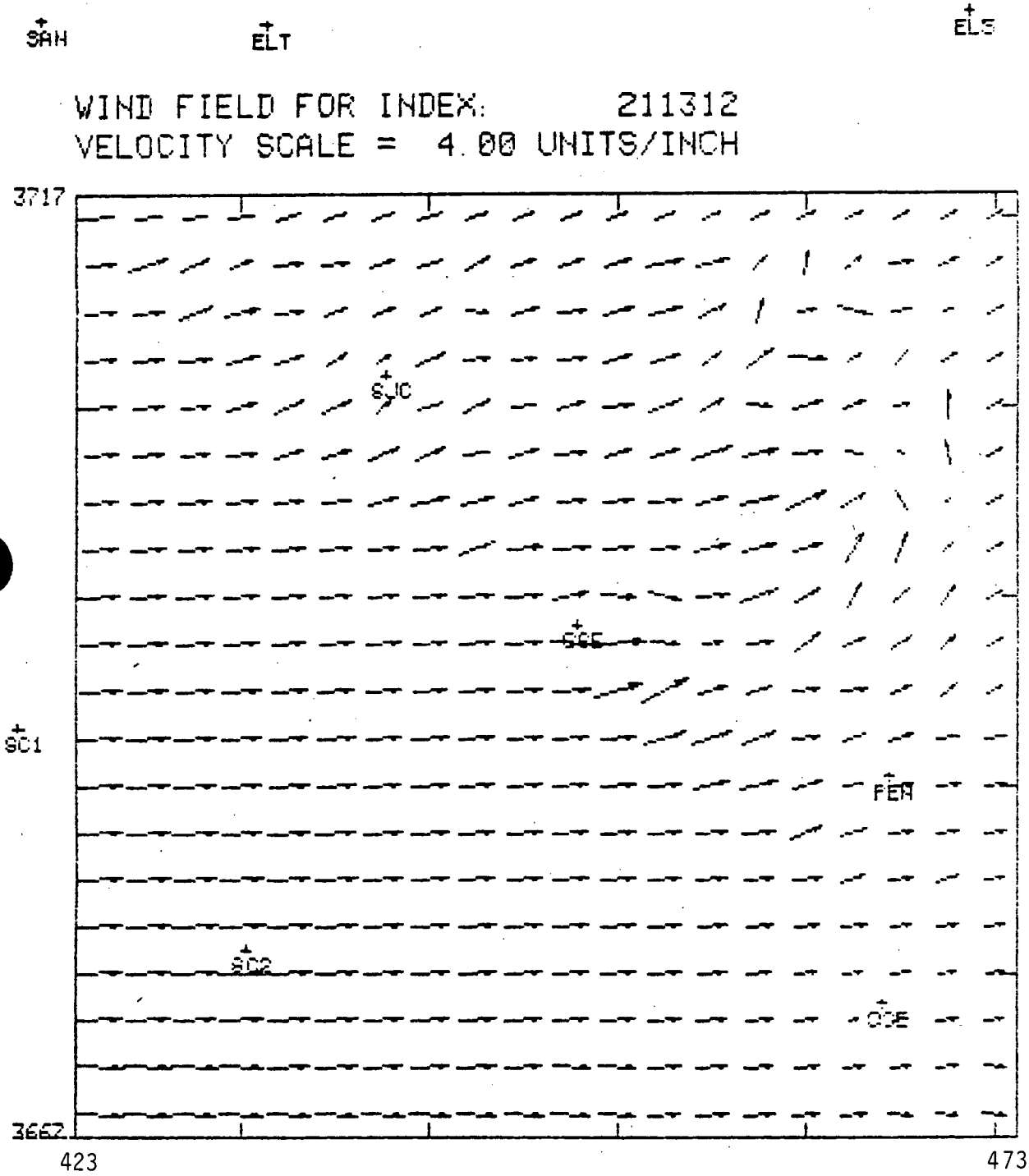

Figure 4-2. A Typical Wind Field Plot for Daytime Unstable Onshore Flow.

REFERENCES

Busse, A.D., and J.R. Zimmerman, 1973. User's Guide for the Climatological Disperison Model, EPAS-R4-73-024, Office of Research and Development, U.S. Environmental Protection Agency, December 1973.

Dames & Moore, 1982. User's Manual for MXPROC Program Selection/Post-Processing Algorithm Nonuniform Meteorological Fields, June 1982.

Holzworth, G.C., 1972. Mixing Heights, Wind Speeds, and Potential Urban Air Pollution Throughout the Contiguous United States, AP-101, Office of Air Programs, U.S. Environmental Protection Agency, 1972.

Raynor, G.S., P. Michael, and S. SethuRaman, 1980. Meteorological Measurement Methods and Diffision Models for Use at Coastal Nuclear Reactor Sites, Nuclear Safety, Vol, 21, No. 6 (November-December) 1980.

Ryan, B.C., 1977. A Mathematical Model for Diagnosis and Prediction of Surface Winds in Mountainous Terrain, Journal of Applied Meteorology, Vol. 16, No. 6, 1977.

Turner, D.B., 1964. A Diffusion Model for an Urban Area, Journal of Applied Meteorology, Vol. 3, No. 1, 1964.

U.S. Nuclear Regulatory Commission (USNRC), 1980. Proposed Revision 1 to Regulatory Guide 1.23; Meteorological Programs in Support of Nuclear Power Plants, Office of Standards Development, September 1980.

APPENDIX A

TECHNICAL DESCRIPTION OF WNDSRF

DESCRIPTION OF THE THREE-DIMENSIONAL WIND FIELD PROGRAMS, WNDSRF AND WIND3D

William R. Goodin

May 1981

Dames & Moore

TABLE OF CONTENTS

LIST OF FIGURES

1.0 INTRODUCTION

A key input to most short-term, mesoscale air pollution transport models is an accurately specified, mass-consistent wind field for each hour of the day. Typically, such a wind field is constructed using a multi-step procedure. The steps can be separated into two groups:

1. Interpolation of the irregularly spaced, measured wind data onto a rectangular computational grid; and

2. Use of objective analysis procedures to adjust the wind field so that it satisfies some physical constraint such as minimum divergence.

This report describes the mathematical basis underlying the set of Dames & Moore programs for constructing mesoscale wind fields. It also consolidates in one document discussions of various parts of these programs that have previously appeared in the literature (Liu and Goodin, 1976; Goodin, et. al., 1979; Goodin, et. al., 1980a; Goodin and McRae, 1980). Recent modifications and improvements to the algorithms are also described.

The report provides a description of the program WNDSRF, which constructs a surface wind field from measured data, and a description of the program WIND3D, which uses the surface wind field produced by WNDSRF in its calculations of a full three-dimensional wind field. Each of these programs requires rectangular arrays of terrain heights, surface roughness values and depth of the surface-based mixed layer. The latter is computed using the program DEPTH, which is described in Appendix A.

2.0 CONSTRUCTION OF A SURFACE WIND FIELD USING WNDSRF

2.1 GENERAL OUTLINE OF THE ALGORITHM

Program WNDRSF constructs a surface (10-meter) wind field on a regular grid using scattered wind data from the region of interest. This two-dimensional wind field is mass-consistent, and each computed wind vector reflects local surface roughness, terrain channeling and surface heating. The following steps comprise the basic algorithm:

- Overlay the region of interest with a two-dimensional grid and specify terrain height and surface roughness values;
- Interpolate surface wind data from scattered locations to grid points using local values of surface roughness, atmospheric stability and mixing depth in the calculation;
- Adjust wind vectors based on local diverting effects of the terrain;
- Compute upslope or downslope wind components resulting from heating or cooling along sloping terrain (if appropriate); and
- Reduce anomalous divergence in the wind field using an iterative procedure.

Each of these steps will be discussed in more detail in the following sections.

2.2 WIND DATA INTERPOLATION USING LOCAL SURFACE ROUGHNESS

In a region with significant variations in surface roughness characteristics, the use of a simple scheme to interpolate measured wind vectors onto a grid may not be appropriate. An example of such a situation is the calculation of wind vectors over a bay or lake using wind data measured onshore. Similarly, wind measurements from an urban area may not be representative of nearby rural conditions. As a result, the first step in the wind program, WNDSRF, considers local surface characteristics during the interpolation procedure.

A number of theoretical and experimental studies analyzing the change in wind profile characteristics downwind of a change in surface roughness have appeared in the literature (Bradley, 1968; Mulhearn, 1977). Unfortunately most of these procedures are only applicable to microscale environments and not to distances on the order of kilometers.

The present algorithm first requires construction of a velocity profile above each measurement station. This is accomplished using similarity theory in the near-surface layer (up to Monin-Obukhov height, L) and a logarithmic profile above that. The integral form of the velocity gradient, given by Monin-Obukhov similarity theory, is:

$$u(z) = u(z_r) + \frac{u_*}{k} \int_{z_r}^{z} \phi\left(\frac{z}{L}\right) \frac{dz}{z} \qquad (1)$$

where $\phi(z/L)$ is given by:

$$\phi(z/L) = \begin{cases} 1 + 4.7\ (z/L) & ;z/L > 0 \\ 1 & ;z/L = 0 \\ [1 - 15\ (z/L)]^{1/4} & ;z/L < 0 \end{cases} \qquad (2)$$

and u_* is the friction velocity, k is the von Karman constant, and z_r is a reference height (usually 10 meters).

Given the ϕ functions, Eq. (1) can be integrated from the reference height, z_r, to z to give:

$$u(z) = \begin{cases} \frac{u_*}{k} \ln(z/z_r) + \ln \frac{\phi_m(z_r/L)^2 + 1)\ (\phi_m(z_r/L) + 1)^2}{\phi_m(z/L)^2 + 1)\ \ (\phi_m(z/L)\ \ + 1)^2} \\ \qquad + 2 \arctan\ (\phi_m(z/L)) \\ \qquad - \arctan\ (\phi_m(z_r/L))\ \ + u_r & ;\ z/L < 0 \\ \frac{u_*}{k} \ln\ (z/z_r) + u_r & ;\ z/L = 0 \\ \frac{u_*}{k} \ln(z/z_r) + \frac{4.7\ (z - z_r)}{L}\ \ + u_r & ;\ z/L > 0 \end{cases} \tag{3}$$

The stable and unstable wind profiles are assumed to apply up to the Monin-Obukhov height. Under neutral conditions, L is infinite and is thus no longer a suitable measure of the depth of the surface layer. As an alternative, the surface layer is often assumed to extend to $z = 0.03\ u_*/f$ (100 m) (Tennekes, 1973). However if the surface friction velocity is used rather than local friction velocity, then the wind profile appears to follow the logarithmic law to greater heights (Panofsky, 1972). Therefore for neutral conditions, the simple logarithmic law is used up to the top of the mixed layer in this study. Above the top of the mixed layer, the velocity is held constant with height.

For stable conditions above the surface layer ($z > L$) a logarithmic profile is used (Webb, 1970). At $z = L$, this profile is matched to the similarity solution so that the gradient is continuous. The resulting equation is:

$$u = \frac{5.7\ u_*}{k} \ln (z/L) + u_L \qquad z > L \quad (4)$$

where u_L is the velocity at $z = L$ computed from Eq. (3c). Above the mixed layer the velocity is assumed to be constant with height.

Similarly, for unstable conditions a logarithmic profile is matched to the similarity solution at $z = L$. The resulting expression is:

$$u = \frac{0.5\ u_*}{k} \ln (-z/L) + u_L \qquad z > -L \quad (5)$$

where u_L is the velocity at $z = L$ computed from Eq. (3a). The velocity is assumed to be constant with height above the mixed layer (or scale height). Procedures for calculating L, u_*, and z_o are presented in Appendix B.

For a smoothly varying field of data, Goodin, et. al. (1979) showed that the inverse-distance-squared weighting ($1/R^2$) interpolation algorithm is accurate, inexpensive and easy to implement. This algorithm is used here to produce a grid of wind vectors at a pre-specified height that is above local surface roughness effects (say 500 meters).

A surface wind vector at each grid point is finally calculated by iteratively converging to a profile that matches the wind vector at the pre-specified height. The advantage to this approach is that the wind profile constructed at each

grid point uses the grid point-specific surface roughness, atmospheric stability and mixing depth.

The algorithm is illustrated in Figure 1. Velocity profiles are first constructed above points labelled 1, 2 and 3. At the height of interest above surface influences the wind vectors are interpolated to the over-water location. The wind profile at that over-water location is then constructed so that it matches the upper-level wind vector.

2.3 CALCULATION OF THE DIVERTING EFFECT OF THE TERRAIN

The second step in the algorithm adjusts the wind field according to the diverting effect of the terrain. The diverting effect of the terrain is assumed to apply only to the direction of the wind, and not its speed. The maximum diversion occurs when the angle between the wind and the aspect of the terrain is 45°. Minimum diversion occurs when the wind is either perpendicular to or parallel to the terrain surface.

The calculation requires the local terrain aspect angle, A (in degrees) and terrain elevation angle, Y (in percent slope). The aspect is the direction that the slope faces, i.e., the horizontal component of the downslope direction. The elevation angle in a particular direction is the slope to the horizon (crest of the terrain) above the location of interest. This number is nonnegative. Eight possible directions from a grid point are used.

The change in wind direction resulting from terrain diversion, $\Delta\theta_{div}$, is computed from:

$$\Delta\theta_{div} = C\ Y \sin(2A-\theta) \qquad (6)$$

where θ is the angle of the incident wind vector (in degrees from north) and C is an empirically determined constant (Ryan,

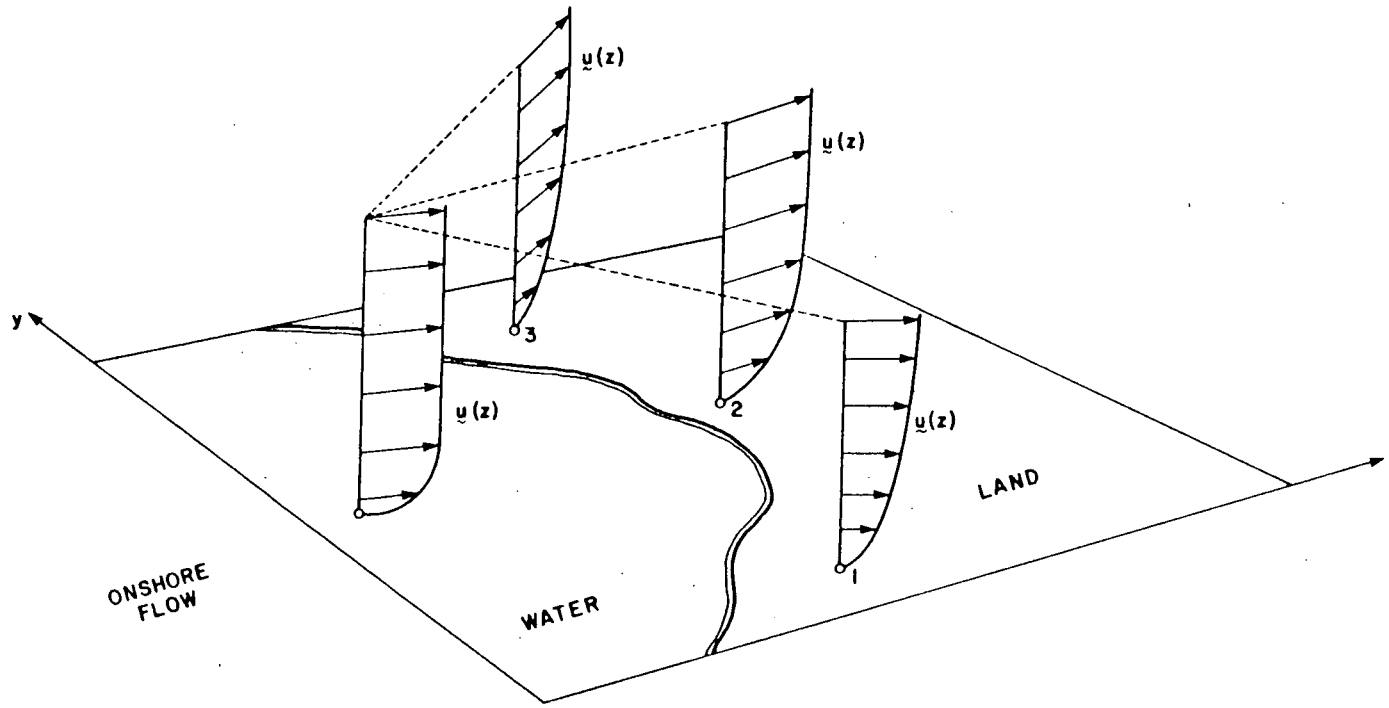

FIGURE 1 WIND PROFILES CONSTRUCTED ABOVE THREE LAND-BASED MEASUREMENT STATIONS AND A LOCATION OVER THE WATER.

1977). The new wind direction at the grid point is obtained by addition of the incident wind direction, θ, and $\Delta\theta_{div}$.

2.4 CALCULATION OF THE SLOPE WIND COMPONENT

Heating (or cooling) of sloping terrain can produce an upslope (or downslope) wind component. The magnitude of the induced wind speed is dependent upon the amount of heating (or cooling), i.e., the number of hours since sunrise (or sunset), the terrain slope, the terrain aspect angle, the ambient air temperature, and the transmission coefficient for the atmosphere.

The program first calculates which type of flow regime might occur. Upslope flow conditions may begin one hour after sunrise and last until sunset. Downslope flow may occur during the other, nighttime hours. The times of sunrise and sunset are computed using the algorithm described in Appendix C.

2.4.1 DOWNSLOPE WIND

The direction of the downslope component vector is opposite to the aspect angle of the terrain at the point of interest. The speed of the wind is computed from:

$$V_{DSLP} = 0.15\ C_{TR}\ \frac{(1 - C_p)}{\tan S} \qquad (7)$$

where:

$$C_p = \exp \frac{-25}{T_{AMB}} (\tan S)^2\ \Delta t \qquad (8)$$

and C_{TR} is the transmission coefficient of the atmosphere, S is the terrain slope (in degrees), T_{AMB} is the ambient

temperature and Δt is the time since sunset plus 2 hours (in hours). The constant 0.15 assumes non-adiabatic cooling of the near-surface layer at the rate of 1.0°C/hour and a lapse rate of 0.5°C/100m. The constant 25 assumes the same lapse rate and a friction coefficient of 0.002 (see Ryan, 1977). The new wind vector at the point of interest is the vector sum of old wind vector and the downslope component vector.

2.4.2 UPSLOPE WIND

The direction of the upslope component vector is the same as the aspect angle of the local terrain. The speed of the upslope wind is computed from:

$$V_{USLP} = \frac{I\ (1 - C_p)}{(697 \tan S)} \qquad (9)$$

and C_p is computed as above except that Δt is the time since sunrise. I is the insolation reaching the terrain surface in W/m^2. The empirical constant 697 is obtained from Ryan (1977).

2.5 SURFACE DIVERGENCE REDUCTION PROCEDURE

Following construction of a gridded wind field from sparse wind measurements, there will certainly be anomalous divergence present in the field. In other words, the two-dimensional continuity equation actually satisfied is:

$$\frac{\partial u}{\partial x} + \frac{\partial v}{\partial y} = D \qquad (10)$$

where D is the anomalous divergence. One could assume that all anomalous divergence in the field is actually vertical motion above the surface layer, i.e., introduce a $\partial w/\partial z$ term

into Eq. (10). However this may cause large vertical velocities at the top of the region of interest since w equals zero at the surface.

The approach used here iteratively reduces the divergence in the surface layer to a specified value by satisfying the continuity equation exactly at each grid point. Eq. (10) is written in finite difference form at point (i,j) as:

$$D^n_{i,j} = (u^n_{i+1,j} - u^n_{i-1,j})/2\ \Delta x + (v^n_{i,j+1} - v^n_{i,j-1})/2\ \Delta y \qquad (11)$$

The superscript n denotes the value of a quantity at the nth iteration; the grid sizes Δx and Δy are assumed constant throughout the domain of computation. To remove the divergence at grid point (i,j), adjustments are made to the u components at (i-1,j) and (i+1,j) grid points. These adjustments to u are equal and of opposite sign. Similar adjustments are made to v at (i,j+1) and (i,j-1) grid points. However, adjustments made at these four points surrounding (i,j) would, in turn, alter the divergence at adjacent points. Thus, the whole grid must be scanned iteratively in order to uniformly reduce the divergence at all locations. The velocities at the (n+1)st iteration will be the values at the nth iteration together with the velocity adjustments $\tilde{u}^n_{i,j}$ and $\tilde{v}^n_{i,j}$. In other words,

$$\begin{aligned} u^{n+1}_{i+1,j} &= u^n_{i+1,j} + f_{i+1,j}\tilde{u}^n_{i,j} \\ u^{n+1}_{i-1,j} &= u^n_{i-1,j} - f_{i-1,j}\tilde{u}^n_{i,j} \\ v^{n+1}_{i,j+1} &= v^n_{i,j+1} + f_{i,j+1}\tilde{v}^n_{i,j} \\ v^{n+1}_{i,j-1} &= v^n_{i,j-1} - f_{i,j-1}\tilde{v}^n_{i,j} \end{aligned} \qquad (12)$$

the value of zero at a station and unity at a non-station. Substitution of Eq. (12) into Eq. (11) yields:

$$(f_{i+1,j} + f_{i-1,j})\tilde{u}^n_{i,j}/2\Delta x + (f_{i,j+1} + f_{i,j-1})\tilde{v}^n_{i,j}/2\Delta y + D^n_{i,j} = 0 \qquad (13)$$

If the first two terms in Eq. (13) are assumed to contribute equally to the divergence, $D^n_{i,j}$,

$$\tilde{u}^n_{i,j} = -D^n_{i,j}\Delta x/(f_{i+1,j} + f_{i-1,j})$$
$$\tilde{v}^n_{i,j} = -D^n_{i,j}\Delta y/(f_{i,j+1} + f_{i,j-1}) \qquad (14)$$

Thus, the solution procedure is as follows. The divergence $D^n_{i,j}$ at the nth iteration is first calculated from Eq. (11), $\tilde{u}^n_{i,j}$ and $\tilde{v}^n_{i,j}$ are then computed using Eq. (14), and finally the values of $u^{n+1}_{i,j}$ and $v^{n+1}_{i,j}$ are obtained by Eq. (12). This procedure is repeated until the divergence is less than a specified value. At the boundary, the velocity components must be prescribed.

This formalism is neither restricted to a four-point finite difference scheme to represent the divergence $D^n_{i,j}$, (Eq. (11)), nor confined to the usage of the immediately adjacent points to carry the full weight of the adjustments at one iteration, (Eq. (12)). In general, the accuracy of the finite difference approximations and the weighting of $\tilde{u}^n_{i,j}$ on $u^n_{i,j}$ may be altered. Eq. (11) can be rewritten to include the values of u and v at eight grid points;

$$D^n_{i,j} = c(u^n_{i+1,j} - u^n_{i-1,j})/2\Delta x$$

$$+ (1 - c)(u^n_{i+2,j} - u^n_{i-2,j})/4\Delta x$$

$$+ c(v^n_{i,j+1} - v^n_{i,j-1})/2\Delta y \qquad (15)$$

$$+ (1 - c)(v^n_{i,j+2} - v^n_{i,j-2})/4\Delta y$$

Eq.(15) is reduced to the four-point approximation when the parameter c assumes the value of unity; Eq. (15) represents a fourth-order accurate scheme when c = 4/3. With the inclusion of c, the velocity adjustments $\tilde{u}^n_{i,j}$ and $\tilde{v}^n_{i,j}$ become:

$$\tilde{u}^n_{i,j} = -2D^n_{i,j}\Delta x/[c(f_{i+1,j} + f_{i-1,j} + f_{i,j+1}$$

$$+ f_{i,j-1}) + \tfrac{1}{2}(1 - c)(f_{i+2,j} + f_{i-2,j} + f_{i,j+2}$$

$$+ f_{i,j-2})] \qquad (16)$$

$$\tilde{v}^n_{i,j} = -2D^n_{i,j}\Delta y/[c(f_{i+1,j} + f_{i-1,j} + f_{i,j+1}$$

$$+ f_{i,j-1}) + \tfrac{1}{2}(1 - c)(f_{i+2,j} + f_{i-2,j} + f_{i,j+2}$$

$$+ f_{i,j-2})]$$

The solution procedure in this more general case is exactly the same as before. The success of this iterative procedure hinges on the systematic reduction of the divergence, $D^n_{i,j}$, and the convergence of $u^n_{i,j}$, $v^n_{i,j}$ as n increases. Proof of the convergence properties of the algorithm are discussed in Liu and Goodin (1976). The results of the interpolation and divergence reduction procedure are shown in Figure 2.

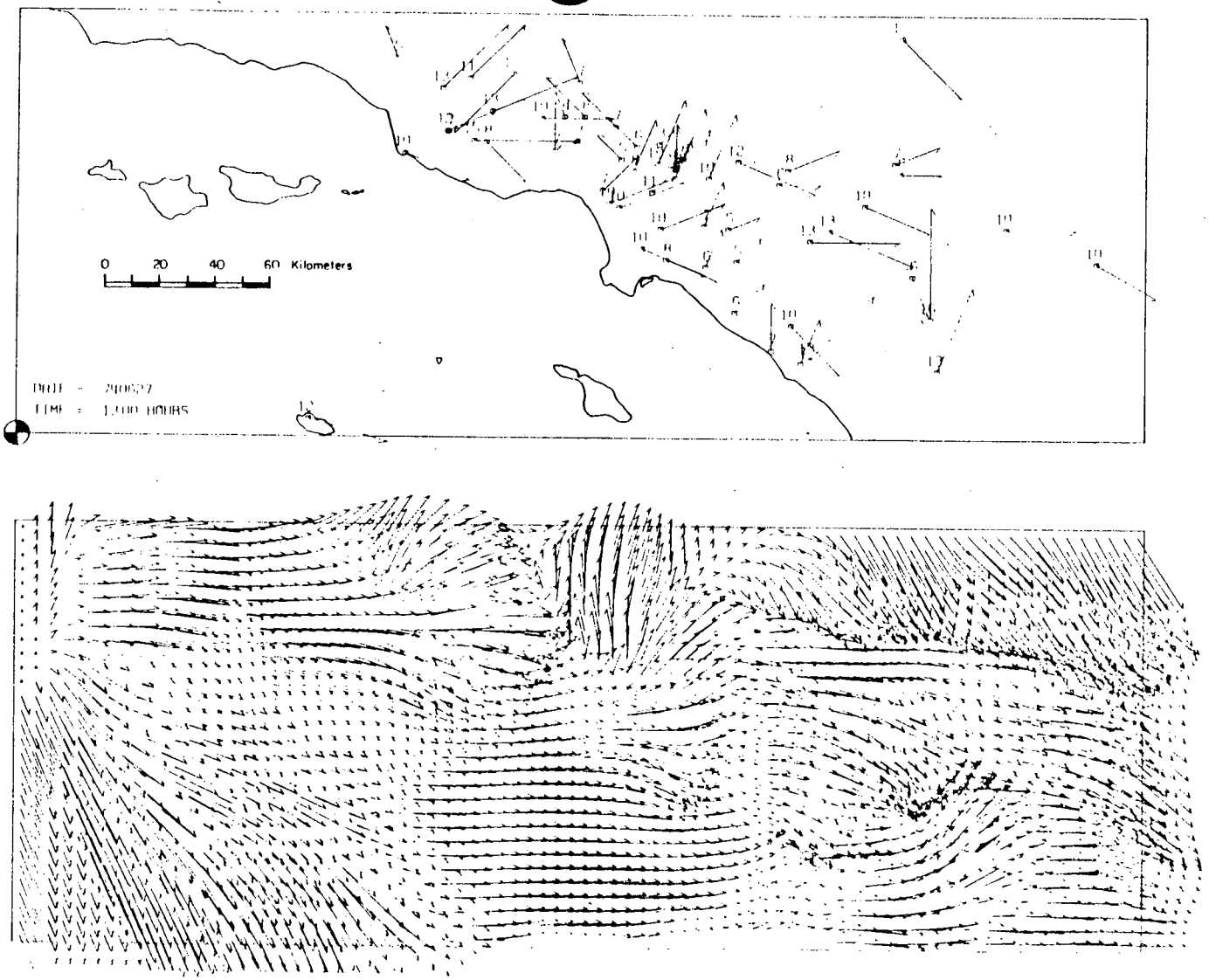

FIGURE 2 HORIZONTAL FLOW FIELD GENERATED BY THE OBJECTIVE ANALYSIS PROCEDURE (LENGTH OF VECTOR IS PROPORTIONAL TO WIND SPEED).

3.0 CONSTRUCTION OF A THREE-DIMENSIONAL WIND FIELD USING WIND3D

3.1 GENERAL OUTLINE OF THE ALGORITHM

Program WIND3D constructs a three-dimensional wind field from sparse measured wind data. The program uses the surface wind field constructed by WNDSRF and the mixing depth field constructed by DEPTH in its calculations. The following steps comprise the algorithm:

- Establish the top of the modeling region and the height of each of the layers within the region;
- Specify the height below which the wind vectors will be calculated using a surface-based wind profile. Above this height measured data will be provided;
- Interpolate the measured and calculated upper-air data from the scattered locations to grid points; and
- Reduce anomalous divergence in the wind field using a three-dimensional iterative procedure.

Each of these steps will be discussed in more detail in the following sections.

3.2 SPECIFICATION AND INTERPOLATION OF WIND VECTORS ALOFT

Once the height of the region of interest has been established (1500 meters is a typical value), the heights of each of the layers must be specified. Five layers are sufficient for most applications. The thickness of the

layers need not be the same, so that layers near the ground can be more closely spaced.

WIND3D allows the user to include as much or as little measured wind data as he desires. If no wind data are available, the program will construct wind profiles above each specified measuring station using the algorithm described in Section 2.2 and Appendix B. The user may also specify that this procedure is to be used to construct vectors in only the lowest layers, and that actual measured data are to be used in the top most layers.

In either case the measured data are first interpolated temporally assuming a linear change between hours. At each hour the measured data are interpolated horizontally using inverse-distance (1/R) weighting of the measurements. Although this interpolation procedure is less accurate than $1/R^2$ interpolation, the errors are of the same order as those that exist in upper-level wind measurements.

To eliminate the difficulty in specifying vertical boundary conditions, a coordinate system that follows the terrain surface was chosen rather than sea level-based coordinates. The transformation from sea level to terrain-following coordinates produces a new vertical velocity, W, i.e.:

$$W = w - u\frac{\partial h}{\partial x} + \rho\frac{\partial \Delta H}{\partial x} - v\frac{\partial h}{\partial y} + \rho\frac{\partial \Delta H}{\partial y} - \rho\frac{\partial \Delta H}{\partial t} \qquad (17)$$

where $\Delta H(x,y,t) = H(x,y,t) - h(x,y)$ is the height of the top of the region above the terrain surface, and ρ is the new vertical coordinate ($0 \leq \rho \leq 1$).

Fig. 3a shows the general case where ΔH is a function of space as well as time. In order to eliminate complications

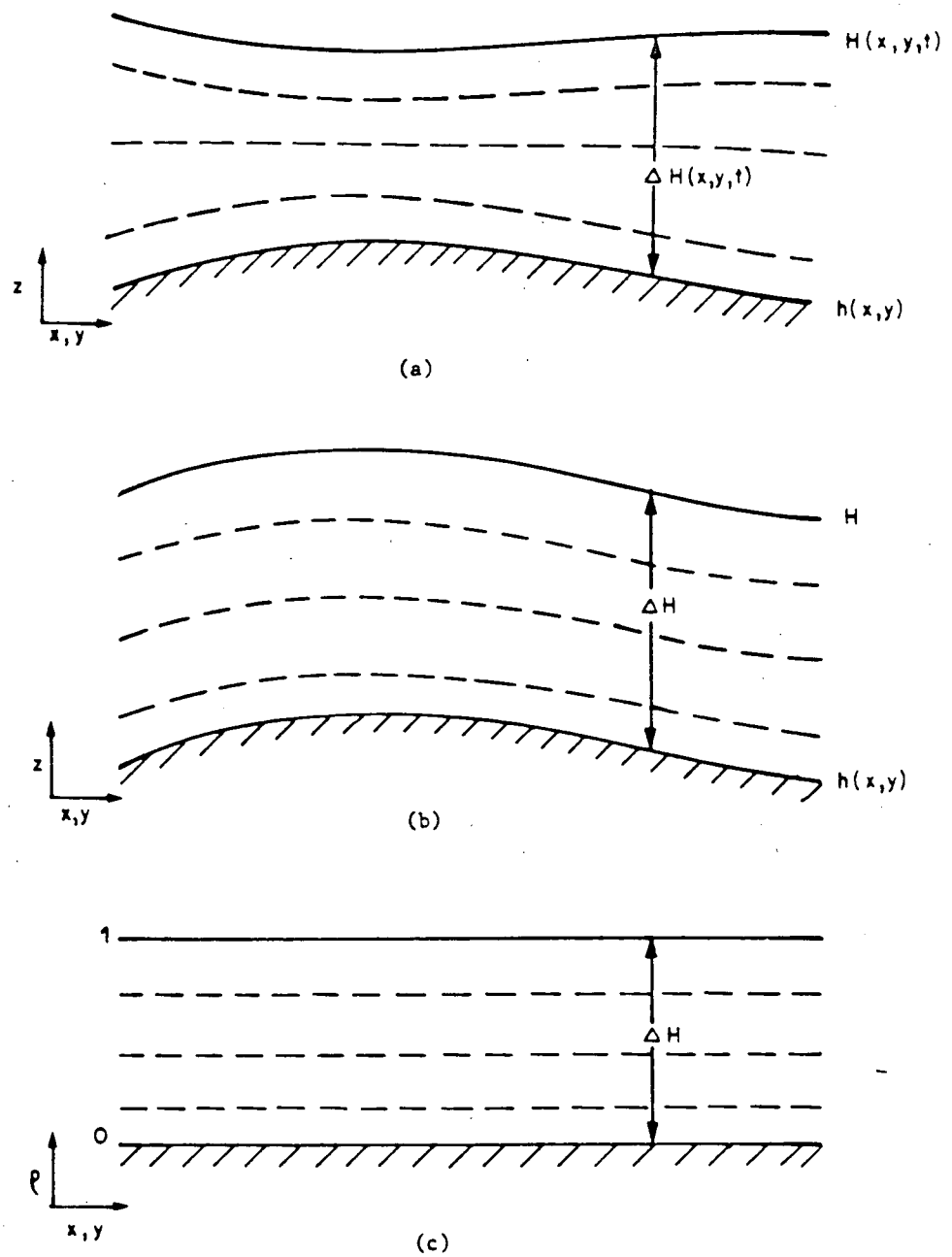

FIGURE 3 A TERRAIN-FOLLOWING COORDINATE SYSTEM: (a) GENERAL CASE H=H(x,y,t); (b) H IS A CONSTANT HEIGHT ABOVE THE TERRAIN; (c) TRANSFORMED x,y,ρ COORDINATE SYSTEM.

introduced into the advection scheme by nonparallelopiped grid volumes in x,y,z-space, H is used for normalization. Figs. 3b and 3c show the transformation from the x,y,z-space to x,y,ρ-space.

In the new coordinate system, the continuity equation is:

$$\frac{\partial W}{\partial \rho} + \frac{\partial(u\Delta H)}{\partial x} + \frac{\partial(v\Delta H)}{\partial y} = 0 \qquad (18)$$

From the interpolated horizontal velocities at each vertical level, W can be calculated using Eq. (18). Unfortunately, this simple solution produces unrealistically large values of W at the top of the region since all residual divergence in the field is propagated upward. Therefore, a procedure is required that will reduce the divergence in the flow field to an acceptable level while maintaining small vertical velocities aloft.

3.3 THREE-DIMENSIONAL DIVERGENCE REDUCTION PROCEDURE

Once the surface level flow field has been established and the upper-level wind data have been interpolated to the three-dimensional grid, the next step is to reduce the divergence in the total flow field. The proposed procedure involves three steps:

1. The divergence is first reduced in each of the interpolated u and v fields at each vertical level (above the surface layer) using a slightly modified version of a simple five-point filter. The equation for smoothing is:

$$u_{i,j}^{n+1} = .020(u_{i,j}^{n} + u_{i+1,j}^{n} + u_{i-1,j}^{n}$$

$$+ u_{i,j+1}^{n} + u_{i,j-1}^{n})(1 - \alpha_k) + \alpha_k u_{i,j}^{n} \qquad (19)$$

where α_k is a parameter that allows the user to keep the measured velocity at station k fixed ($\alpha_k = 1$) or keep only some of its original influence ($\alpha_k < 1$). This parameter is zero at all non-measuring station points. This first step is designed to reduce as much of the anomalous divergence as possible. The more smoothing a field of wind components is subjected to, the more initial anomalous divergence is dissipated horizontally within that layer, i.e., the smaller will be the vertical velocity above it.

2. Following this initial smoothing step, the vertical velocity above each layer is computed from the divergence within the layer. The layers are temporarily disconnected from each other during this calculation so that the calculated vertical velocity above a layer depends only upon the divergence within it. This prevents velocities at the top of the region from becoming unrealistically large. These vertical velocities will be held fixed throughout the rest of the divergence reduction procedure; and

3. The final refinement reduces the remaining divergence that exists within each layer by application of a two-dimensional technique similar to that of Liu and Goodin (1976). The equation solved is (with ΔH = constant).

$$\frac{\partial W}{\partial \rho} + \Delta H \left(\frac{\partial u}{\partial x} + \frac{\partial v}{\partial y}\right) - D_R\ (x,y,\rho) \qquad (20)$$

where $D_R\ (x,y,\rho)$ is a measure of the remaining divergence. At grid point (i,j,k), Eq. (20) can be written as:

$$D_{ijk}^{n+1} = \frac{W_{i,j,k+1/2} - W_{i,j,k-1/2}}{\Delta\rho}$$

$$+ H \frac{u_{i+1/2,j,k}^{n+1} - u_{i-1/2,j,k}^{n+1}}{\Delta x}$$

$$+ \frac{v_{i,j+1/2,k}^{n+1} - v_{i,j-1/2,k}^{n+1}}{\Delta y} \qquad (21)$$

where the superscript n+1 indicates that the values are computed for the (n+1)st iteration, and the subscript R is dropped from D_R for convenience.

To remove the divergence at the point (i,j,k), adjustments are made to the u values at (i + 1/2,j,k,) and (i-1/2,j,k). Similar adjustments are made to v at (i,j + 1/2,k) and (i,j - 1/2,k) in order that the divergence is exactly zero at (i,j,k). Since this procedure will add additional divergence to surrounding points, the whole grid must be scanned iteratively. The adjustments to the velocity components are:

$$u_{i+1/2,j,k}^{n+1} = u_{i+1/2,j,k}^{n} + u_t$$

$$u_{i-1/2,j,k}^{n+1} = u_{i-1/2,j,k}^{n} - u_t$$

$$v^{n+1}_{i,j+1/2,k} = v^{n}_{i,j+1/2,k} + v_t$$

$$v^{n+1}_{i,j-1/2,k} = v^{n}_{i,j-1/2,k} - v_t \qquad (22)$$

where u_t and v_t are the adjustment velocities. These velocities are computed by substitution in Eq. (21),

$$0 = D_{ijk} + \Delta H\left(\frac{2u_t}{\Delta x} + \frac{2v_t}{\Delta y}\right) \qquad (23)$$

Assuming that $\Delta y = \Delta x$ and that the velocity adjustments are equally weighted in each direction, Eq. (23) can be solved to give:

$$u_t = \frac{-D_{ijk}\,\Delta x}{4\Delta H} \qquad (24)$$

Thus, the complete three-dimensional divergence reduction procedure consists of:

1) Smoothing of the component fields at each level using an empirically determined number of smoothing passes;

2) Solution of Eq. (21) at each level for $W_{i,j,k+1/2}$, temporarily assuming $W_{i,j,k-1/2}$ is zero; and

3) Solution of Eqs. (21), (24) and (20) repeatedly using the calculated values for W until the maximum divergence is reduced to an acceptable level. The magnitude of the divergence should be less than the local vertical velocity and less than the estimated errors in the horizontal velocity components.

The interaction between the flow field and the change in depth of the mixed layer has not been accounted for in the above procedure because mixing depth and vertical velocity are never measured simultaneously, and because attempts to tie the vertical cell heights to the mixing depth resulted in large horizonal wind velocities as the mixing depth approached zero. An evaluation of the performance of the three-dimensional wind field algorithm is described in Goodin, et. al. (1980a).

4.0 SUMMARY

This report has described the mathematical procedures employed by the programs WNDSRF and WIND3D to construct a mesoscale, three-dimensional wind field from measured wind data. These programs require data that describe the region of interest - terrain heights and surface roughness characteristics, as well as mixing depth and, surface and upper-air and measurements. Anomalous divergence in the resulting wind field is reduced to a user-specified level using an iterative technique. The model is easy to implement, computationally efficient and has been evaluated using measured data from the San Francisco Bay area (Goodin, et. al., 1980b), Los Angeles (Goodin, et. al., 1980a) and Valdez, Alaska (Goodin et. al., 1980b).

REFERENCES

Bradley, E.F. (1968) A micrometeorological study of velocity profiles and surface drag in the region modified by a change in surface roughness, Quart. J. Royal Met. Soc., 94, 351-379.

Businger, J.A., Wyngaard, J.C., Izumi, Y. and Bradley, E.F. (1971) Flux-profile relationships in the atmospheric surface layer, J. of the Atmospheric Sciences, 28, 181-189.

Golder, D. (1972) Relations among stability parameters in the surface layer, Boundary Layer Meterorology, 3, 47-58.

Goodin, W.R., McRae, G.J. and Seinfeld, J.H. (1979) A comparison of interpolation methods for sparse data: application to wind and concentration fields, J. Appl. Met., 18, 761-771.

Goodin, W.R., and McRae, G.J. (1980). A procedure for wind field construction from measured data that utilizes local surface roughness, Proc. of Second Conference on Coastal Meteorology, Amer. Met. Soc., Los Angeles, California, 233-239.

Goodin, W.R, A.K. Runchal and G.Y. Lou (1980b). Evaluation and Application of the Random-walk Advection and Dispersion Model (RADM), Symposium on Intermediate-Range Atmospheric Transport Processes and Technology Assessment, DOE/NOAA/ORNL, Gatlinburg, TN.

Goodin, W.R., McRae, G.J., and Seinfeld, J.H. (1980a) An objective analysis technique for constructing three-dimensional, urban-scale wind fields, J. Appl. Met., 19, 98-108.

Hodgin, C.R. (1980) Logarithmic wind profile parameters applied to air quality assessment studies, Proceedings Second Joint Conference on Applications of Air Pollution Meterology, AMS/APCA, New Orleans, LA., 770-776.

List, R.J. (1971) Smithsonian Meteorological Tables, Smithsonian Institution Press, Washington, D.C., 527 pp.

Liu, C.Y. and W.R. Goodin (1976) An iterative algorithm for objective and field analysis, Mon. Wea. Rev., 104, 784-791.

REFERENCES (Continued)

Liu, M.K. et al. (1976) The chemistry, dispersion and transport of air pollutants emitted from fossil fuel power plants in California: data analysis and emission impact model, EF76-18R, Systems Applications, Inc. San Rafael, California, 245 pp.

Monin, A.S. and Obukhov, A.M. (1954) Basic laws of turbulent mixing in the ground layer of the atmosphere, Geophys. Inst. Acad. Sci. USSR, 24, 163-187.

Mulhearn, P.J. (1977) Relations between surface fluxes and mean profiles of velocity, temperature and concentration, downwind of a change in surface roughness, Quart, J. Royal Met. Soc., 103, 785-802.

Panofsky, H.A., (1972) Tower micrometeorology, in Workshop on Micrometeorology, D.A. Haugen: ed., Amer. Met. Soc., Boston, Massachusetts, 151-167.

Ryan, B.C. (1977) A mathematical model for diagnosis and prediction of surface winds in mountainous terrain, J. Appl. Met., 16, 571-584.

Tennekes, H. (1973) The logarithmic wind profile, J. Atmos. Sci., 30, 234-238.

Turner, D.B. (1964) A diffusion model for an urban area, J. Appl. Met., 3,83-91.

Uthe, E.E. and W.B. Johnson (1981) Applications of airborne LIDAR to studies of intermediate-range transport and diffusion, Proc. Fifth Symposium on Turbulence, Diffusion and Air Pollution, Amer. Met. Soc., Atlanta, GA.

Webb, E.K. (1970) Profile relationships: the log-linear range, and extension to strong stability, Q.J. Royal Met. Soc., 96, 67-90.

APPENDIX A
CALCULATION OF MIXING DEPTH

A.1 DESCRIPTION OF THE ALGORITHM

When computing pollutant concentrations in a three-dimensional airshed, an important meteorological parameter is the depth of the mixed layer specified as a function of time and space. This parameter, which is used by the wind field calculation programs WNDSRF and WIND3D, is constructed by the program DEPTH. This program calculates the depth of the surface mixed layer above the terrain at each grid point in the region using measured mixing depth data from scattered monitoring locations. These data may be acoustic sounder, tethersonde, aircraft and/or radiosonde measurements. The only requirement is that the raw temperature structure data be converted to heights above sea level prior to input to DEPTH. Only one mixed layer depth at a time is permitted at a given monitor; multiple inversion layers cannot be modeled.

Since the measured data are usually sparse in time as well as space, the program first interpolates the measured data in time, assuming a linear profile between hours. In order to avoid extrapolation in time, the user must specify a mixing depth at each measuring station for the beginning and ending times of the calculation (usually 0000 and 2300).

Once a mixing depth has been computed for each measuring station at each hour of interest, the program computes the mixing depth over the whole region for each hour beginning with the first hour specified. The first step in the calculation is to determine whether daytime or nighttime conditions exist at each grid point. The procedure to do this is

a standard one, involving formulae from List (1971). The slope and aspect of the terrain are included in the calculation. If the sun is above the horizon at that grid point, then it is assumed that the mixed layer follows the terrain contours. This phenomenon has been observed during a number of field studies, especially on south-facing mountain slopes (see, for example, Uthe and Johnson, 1981). The mixing depth at each grid point is interpolated from the measured mixing depths using the following formula:

$$h_{ij} = \left(\sum_{k=1}^{N} h_k/d_k\right)/\left(\sum_{k=1}^{N} 1/d_k\right) \qquad (A.1)$$

where h_{ij} is the mixing depth at grid point (i,j), h_k is the measured mixing depth at measurement station k and d_k is the distance from grid point (i,j) to monitor k.

During nighttime conditions, the top of the mixed layer is assumed to remain constant with respect to sea level due to the general stability of the atmosphere, i.e.,

$$h_{ij} = \left(\sum_{k=1}^{N} (h_k + z_k)/d_k\right)/\left(\sum_{k=1}^{N} 1/d_k\right) - z_{ij} \qquad (A.2)$$

where z_k is the terrain height at measurement station k and z_{ij} is the terrain height of grid point (i,j). The daytime and nighttime situations are illustrated in Figure A.1.

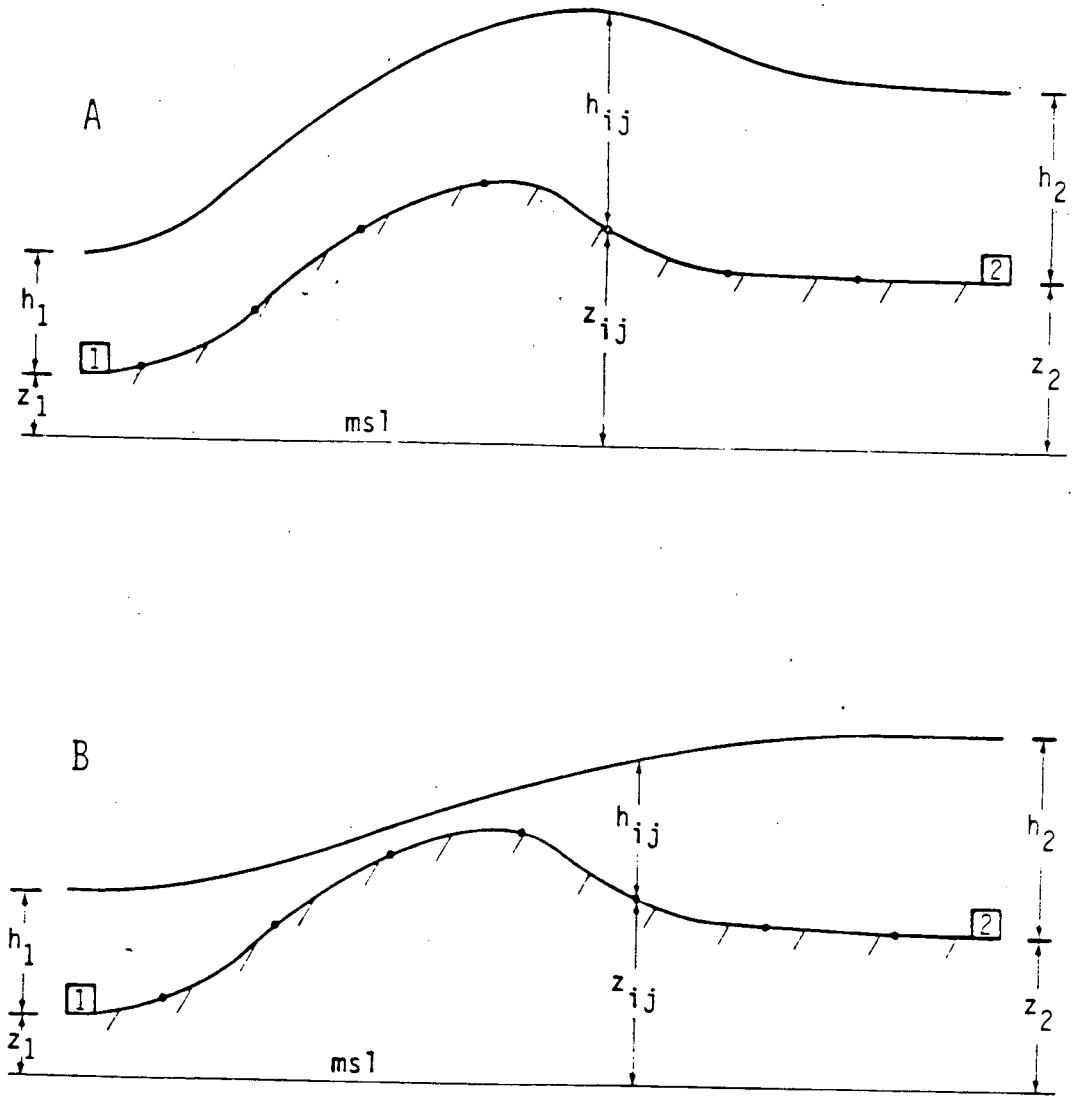

Figure A.1 Cross-sectional view of mixed layer interpolated from measured heights at two monitors, labelled 1 and 2. A) Daytime conditions; B) Nighttime conditions.

APPENDIX B

CALCULATION OF L, u_* and z_o

B.1 PARAMETERS REQUIRED IN WIND PROFILE CALCULATION

The procedure used to calculate the wind profile at each measuring station requires calculation of the Monin-Obukhov length, L, and friction velocity, u_*. The techniques used to calculate these parameters, which are functions of surface roughness and stability, are presented in the following subsections.

B.2 ESTIMATION OF THE MONIN-OBUKHOV LENGTH

The Monin-Obukhov length is a key parameter in the present model. Golder (1972) established a relationship between L, the stability classes of Pasquill and Turner, and the roughness height, z_o. The results of his investigation are shown in Figure B.1. The bounding solid lines on the plots for a particular stability class represent a standard deviation about the mean.

The Turner stability class can be estimated from a knowledge of wind speed, cloud cover and cloud ceiling height (Turner, 1964). The Monin-Obukhov length is then computed from Golder's nomogram as a function of this stability class and z_o. In order to simplify this calculation, each stability class is approximated by a single straight line. The parameters for these straight-line approximations to Golder's nomogram are shown in Table B.1. A similar technique for computing 1/L from Golder's work was discussed by Liu, et. al. (1976).

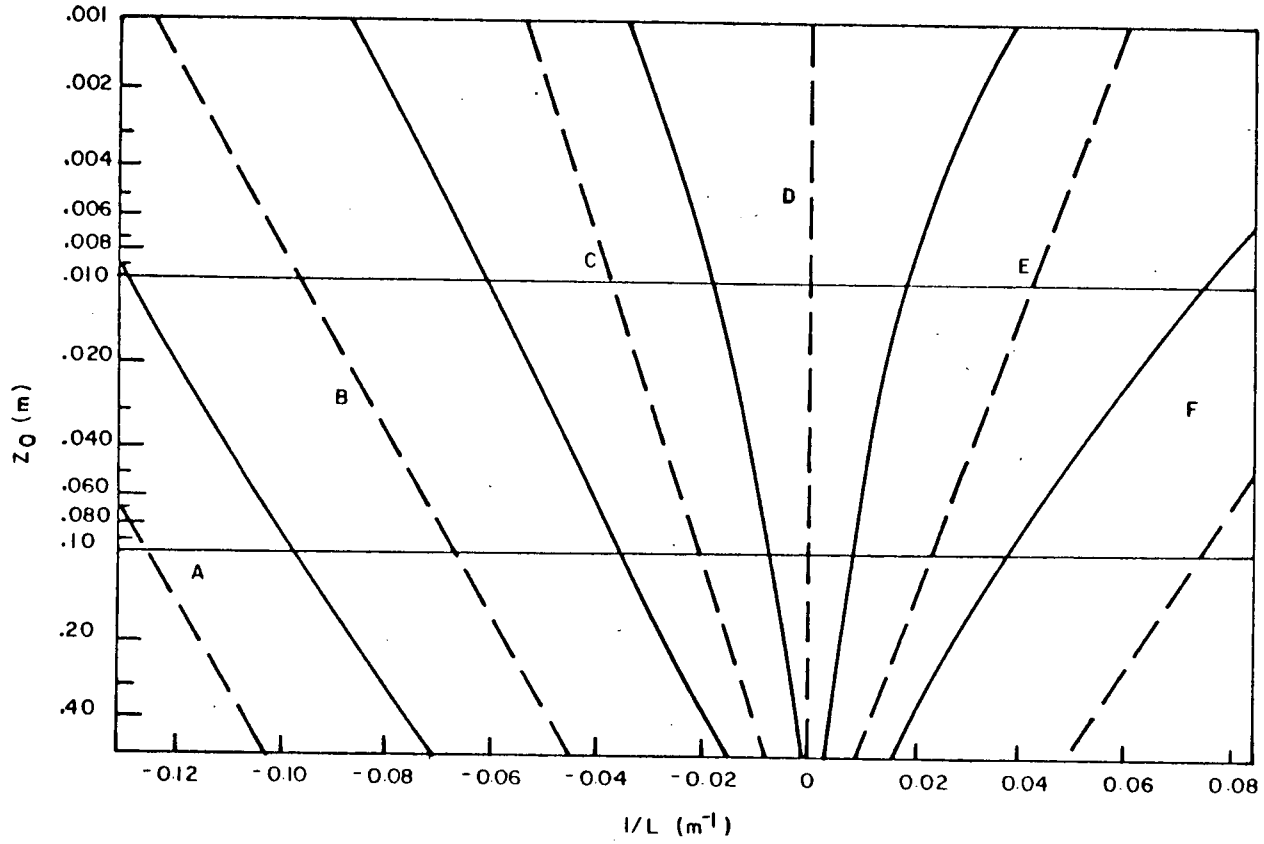

FIGURE B.1 NOMOGRAM SHOWING RELATIONSHIP BETWEEN Z_0, L AND STABILITY CLASS.

TABLE B.1
Coefficients for Straight-Line Approximation to Golder's Plot as a Function of Stability Classes

$$\frac{1}{L} = a + b \log_{10} z_o$$

Turner	Stability Class	Coefficients a	b
Extremely Unstable	A	-0.084	0.026
Moderately Unstable	B	-0.035	0.025
Slightly Unstable	C	-0.008	0.017
Neutral	D	0	0
Slightly Stable	E	+0.005	-0.005
Moderately Stable	F	+0.010	-0.015
Extremely Stable	G	0.045	-0.025

B.3 DETERMINATION OF FRICTION VELOCITY

Close to the ground in the constant flux layer, u_* is a measure of turbulent eddy formation and of the transfer of momentum due to these fluctuations. The friction velocity, u_*, is used in many calculations. This section presents some simple formulae that can be used for its calculation under a variety of meteorological conditions.

The friction velocity is defined by:

$$u_*^2 = \frac{\tau_o}{\rho} = \overline{u'w'} \tag{B.1}$$

where τ_o is the shearing stress per unit area of the boundary and ρ is the density of the fluid. A K-Theory approximation for the momentum flux $\overline{u'w'}$ and a Monin-Obukhov similarity expression can be used to develop the following form

$$u_* = \frac{k\, u(z_r)}{\int_{z_o}^{z_r} \phi_m \frac{z}{L} \frac{dz}{z}} \tag{B.2}$$

where $u(z_r)$ is the velocity at a reference elevation z_r, typically the height of the wind measuring instrument above the surface, L is the Monin-Obukhov length and ϕ_m is a function related to wind shear that must be determined experimentally. The velocity at the height of the momentum sink, z_o, is assumed to be zero.

Businger et al. (1971) developed the following series of ϕ_m functions from field data,

$$\phi_m\left(\frac{z}{L}\right) = \begin{cases} 1 + 4.7\ (z/L) & ;z/L > 0 \\ 1 & ;z/L = 0 \\ [1 - 15\ (z/L)]^{-1/4} & ;z/L < 0 \end{cases} \qquad \text{(B.3)}$$

Substituting these expressions into Eq. (B.3) and integrating gives the following formulae for the friction velocity

$$u_* = \begin{cases} \dfrac{k\ u(z_r)}{\ln \dfrac{1-\phi_m(\frac{z_r}{L})}{1+\phi_m(\frac{z_r}{L})} \ln \dfrac{1-\phi_m(\frac{z_o}{L})}{1+\phi_m(\frac{z_o}{L})} + 2\arctan \dfrac{1}{\phi_m(\frac{z_r}{L})} - 2\arctan \dfrac{1}{\phi_m(\frac{z_o}{L})}} & ; \dfrac{z}{L} < 0 \\ \dfrac{k\ u(z_r)}{\ln(\frac{z_r}{z_o}) + \frac{4.7}{L}(z_r - z_o)} & ; \dfrac{z}{L} > 0 \\ \dfrac{k\ u(z_r)}{\ln(\frac{z_r}{z_o})} & ; \dfrac{z}{L} = 0 \end{cases} \qquad \text{(B.4)}$$

B.4 ESTIMATION OF SURFACE ROUGHNESS

With the present method for estimating L, the effects of small scale surface irregularities on the transfer process in the boundary layer are incorporated only through the surface roughness parameter, z_o. As a result, z_o has to be specified at each grid point within the modeling region. The range of variation of z_o over different land types is quite large and the measurements required to estimate the effective roughness are quite complex.

Figure B.2 presents surface roughness values for a variety of land use categories. These data were compiled by Hodgin (1980) from a variety of sources. The precision implied by the numerical entries in the figure is deceptive; in practice there is considerable scatter.

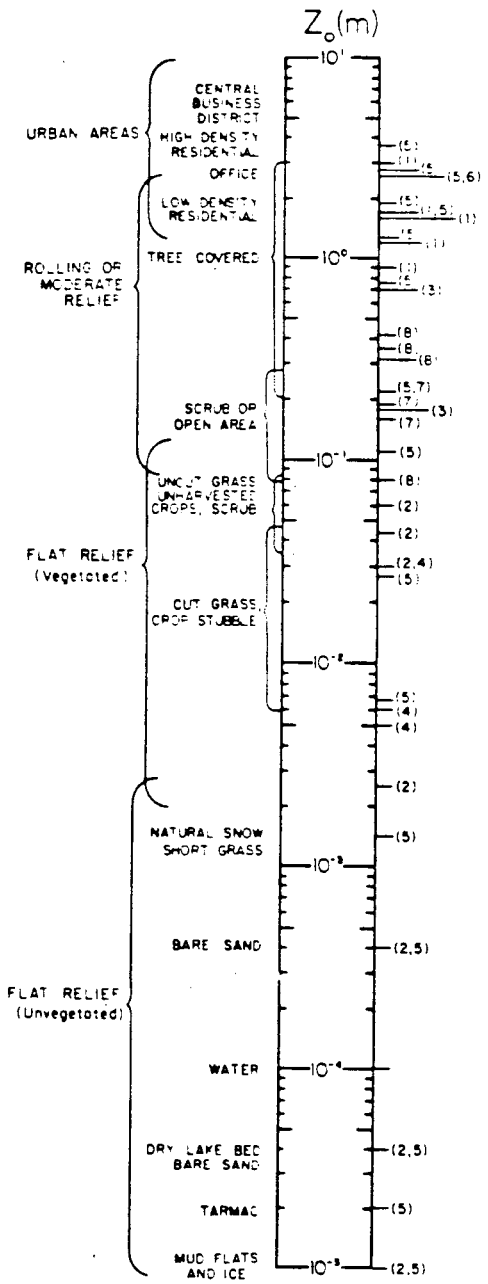

REFERENCES

1 COUNIHAN (1975)
2 DEACON (1949)
3 FICHTL and McVEHIL (1970)
4 GOLDER (1972)
5 MYRUP and RANZIER (1976)
6 SLADE (1969)
7 TOUMA (1977)
8 WEBER et al (1975)

FIGURE B.2 VARIATION OF SURFACE ROUGHNESS AS A FUNCTION OF SURFACE TYPE

APPENDIX C

CALCULATION OF SUNRISE, SUNSET AND SOLAR RADIATION

The slope wind calculation procedure, described in Section 2.4, requires the times of sunrise and sunset to calculate the speed of the wind component. During daylight hours, the magnitude of the solar radiation is also required.

C.1 CALCULATION OF TIMES OF SUNRISE AND SUNSET

The times of sunrise and sunset can be expressed as:

$$t_{sr} = (h_{sr} + 180)/15 - \Delta t_z + L/15 - Q$$

$$t_{ss} = (h_{ss} + 180)/15 - \Delta t_z + L/15 - Q \qquad \text{(C.1)}$$

where h_{sr} and h_{ss} are the hour angles at sunrise and sunset, Δt_z is the time difference from Greenwich mean time, L is the longitude and Q is a time adjustment.

The hour angles are computed from:

$$h_{sr} = -\cos^{-1} (-\sin (0.8 + C_{el} - \tan^{-1} (Y_r)) - \sin \phi \sin \delta)/(\cos \phi \cos \delta)$$

$$h_{ss} = \cos^{-1} (-\sin (0.8 + C_{el} - \tan^{-1}(Y_s)) - \sin \phi \sin \delta)/(\cos \phi \cos \delta) \qquad \text{(C.2)}$$

where ϕ is the latitude, δ is the declination of the sun, C_{el} is a correction for elevation (earth curvature) and Y_r and Y_s are the elevation angles to the horizontal at the azimuth of the sun at sunrise and sunset. The elevation correction is computed from:

$$C_{el} = \cos^{-1} (6.37 \times 10^6/(6.37 \times 10^6 + 1.32\ Z_s)) \quad (C.3)$$

where Z_s is the terrain height. The elevation angles are computed from:

$$Y_r = 90 + (21.0 + 1.4 \exp(\phi)/19.0) \cos (0.986\ d + 7.9)$$

$$Y_s = 270 - (21.0 + 1.4 \exp(\phi)/19.0) \cos (0.986\ d + 7.9) \quad (C.4)$$

where d is the Julian day. The declination of the sun is computed from:

$$\delta = 23.45 \sin (0.973\ (d - 81.5)) \quad (C.5)$$

The time adjustment is computed from:

$$Q = (0.7 \sin (-0.986\ d) + \sin (-1.971\ d - 15.78))/6.0 \quad (C.6)$$

C.2 CALCULATION OF SOLAR RADIATION

If the hour of interest is between sunrise and sunset, the insolation in watts per square meter can be computed from:

$$I = 1350\ P \exp(1/\sin C) \sin \xi \quad (C.7)$$

where P is the transmissivity, C is altitude of the sun, and ξ is the angle at which the sun's radiation strikes the slope at time t.

The altitude of the sun is computed from:

$$C = \sin^{-1} (\cos \phi \cos h \cos \delta + \sin \phi \sin \delta) \qquad (C.8)$$

The angle ξ is computed from:

$$\xi = \sin C \cos S + \cos C \sin S \cos (Z - A) \qquad (C.9)$$

where S is the slope of the terrain, Z is the azimuth angle f the sun, and A is the aspect angle of the terrain.

The azimuth angle of the sun is:

$$Z = \sin^{-1} (-\cos \delta \sin h / \cos C) \qquad (C.10)$$